

*This article is a non-reviewed preprint published at EarthArXiv and was submitted to Marine Geology for peer-review.*

**Tracing marine cryptotephra in the North Atlantic during the Last Glacial Period: Identification, characterisation and depositional controls**

Peter M. Abbott<sup>1,2,3,\*</sup>, Adam J. Griggs<sup>1</sup>, Anna J. Bourne<sup>1,4</sup>, Siwan M. Davies<sup>1</sup>

<sup>1</sup>Department of Geography, College of Science, Swansea University, Singleton Park, Swansea, SA2 8PP, UK

<sup>2</sup>School of Earth and Ocean Sciences, Cardiff University, Park Place, CF10 3AT, Cardiff, UK

<sup>3</sup>Institute of Geological Sciences and Oeschger Center for Climate Change Research, University of Bern, Baltzerstrasse 1+3, Bern 3012, Switzerland

<sup>4</sup>Geography and Environment, University of Southampton, University Road, Southampton, SO17 1BJ, UK

\*Corresponding author (abbottp@cardiff.ac.uk)

1 **Tracing marine cryptotephra in the North Atlantic during the Last Glacial Period:**  
2 **Identification, characterisation and depositional controls**

3

4 Peter M. Abbott<sup>1,2,3,\*</sup>, Adam J. Griggs<sup>1</sup>, Anna J. Bourne<sup>1,4</sup>, Siwan M. Davies<sup>1</sup>

5

6 <sup>1</sup>Department of Geography, College of Science, Swansea University, Singleton Park,

7 Swansea, SA2 8PP, UK

8 <sup>2</sup>School of Earth and Ocean Sciences, Cardiff University, Park Place, CF10 3AT, Cardiff, UK

9 <sup>3</sup>Institute of Geological Sciences and Oeschger Center for Climate Change Research,

10 University of Bern, Baltzerstrasse 1+3, Bern 3012, Switzerland

11 <sup>4</sup>Geography and Environment, University of Southampton, University Road, Southampton,

12 SO17 1BJ, UK

13

14 \*Corresponding author (abbottp@cardiff.ac.uk)

15

16 ***Abstract***

17

18 Tephrochronology is increasingly being utilised as a key tool for improving chronological

19 models and correlating disparate palaeoclimatic sequences. For many sedimentary

20 environments, however, there is an increased recognition that a range of processes may

21 impart a delay in deposition and/or rework tephra. These processes can affect the integrity of

22 tephra deposits as time-synchronous markers, therefore, it is crucial to assess their

23 isochronous nature, especially when cryptotephra are investigated in a dynamic marine

24 environment. A methodology for the identification and characterisation of marine

25 cryptotephra alongside a protocol for assessing their integrity is outlined. This was applied

26 to a wide network of North Atlantic marine sequences covering the last glacial period. A  
27 diverse range of cryptotephra deposits were identified and based on similarities in physical  
28 characteristics, indicative of common modes of tephra delivery and post-depositional  
29 reworking, a deposit type classification scheme was defined. The presence and dominance of  
30 different deposit types within each core allowed an assessment of spatial and temporal  
31 controls on tephra deposition and preservation. Overall, isochronous horizons can be  
32 identified across a large portion of the North Atlantic due to preferential atmospheric  
33 dispersal patterns. However, the variable influence of ice-rafting processes and an interplay  
34 between the high eruptive frequency of Iceland and relatively lower sedimentation rates can  
35 also create complex tephrostratigraphies in this sector. We show that sites within a wide  
36 sector to the south and east of Iceland have the greatest potential to be repositories for  
37 isochronous horizons that can underpin or facilitate the synchronisation of palaeoclimatic  
38 records.

39

40 **Keywords:** Quaternary; palaeoceanography; tephrochronology; North Atlantic; transport and  
41 deposition; marine cores

42

### 43 ***1. Introduction***

44

45 Deposits of volcanic ash, tephra, can act as time-synchronous marker horizons linking  
46 palaeoclimatic sequences to help improve chronological models and assess the relative timing  
47 of climatic changes (Lowe, 2011). Two fundamental principles that underpin the application  
48 of tephrochronology are the rapid deposition of ash at all sites, i.e. instantaneous in  
49 geological terms, and that the stratigraphic position of the ash in a sequence directly relates to  
50 the timing of the volcanic eruption. Processes that either delay the transportation of ash

51 particles to a site or rework the material following initial deposition can have major impacts  
52 on the integrity of deposits as well-resolved isochronous markers. The operation of such  
53 processes has been investigated in many sedimentary environments (e.g. Ruddiman and  
54 Glover, 1972; Austin et al., 2004; Davies et al., 2007; Brendryen et al., 2010; Payne and  
55 Gehrels, 2010; Pouget et al., 2014; Todd et al., 2014; Watson et al., 2015) and are particularly  
56 crucial for cryptotephra, due to the absence of any visible stratigraphic features that would  
57 identify the position of the isochron and hence the timing of deposition and draw attention to  
58 any post-depositional reworking (Davies, 2015). For the marine environment it is critical to  
59 consider these processes due to its dynamic nature and the wide range of potential influences,  
60 especially when investigating sediments from glacial periods and high-latitude settings where  
61 ice-rafting processes could be a significant complicating factor.

62

63 Isochronous tephra deposits are formed in the marine environment if primary tephra fallout is  
64 deposited on the ocean surface, rapidly transported through the water column, deposited on  
65 the seabed and then preserved in the sediment by subsequent marine sedimentation (Figure  
66 1). However, deposition onto other surfaces, e.g. ice sheets and sea-ice, subsequent rafting,  
67 and post-depositional reworking and redistribution processes, such as bioturbation and  
68 sedimentary loading, can have a major impact on the integrity of tephra deposits in this  
69 environment (Figure 1). For instance, these processes can affect the stratigraphic position of a  
70 tephra, a pertinent issue for marine sequences due to their lower resolution relative to other  
71 records, and potentially compromise the use of the deposit as an isochron. As such, it is  
72 essential that a full assessment of the sedimentation and depositional processes influencing  
73 the preservation, form and isochronous nature of marine cryptotephra deposits is undertaken.  
74 This is especially important if tephra horizons are to be used as tie lines to assess the relative  
75 timing of climatic changes between depositional environments.



76

77 Here we present an optimised protocol for marine cryptotephra studies. Our examples are  
78 derived from a range of depositional settings in the North Atlantic region (Figure 2), but the  
79 methodological approach could be applicable to many other marine settings. Within our  
80 approach, cryptotephra are identified and characterised using density separation, magnetic  
81 separation and electron probe micro-analysis (EPMA) techniques. We then employ a series of  
82 indicators to assess the isochronous nature of tephra deposits in the North Atlantic. These  
83 include (i) high-resolution shard concentration profiles, (ii) glass shard size variations, (iii)  
84 comprehensive single-shard geochemical analysis, and (iv) when available co-variance with  
85 ice-rafted debris (IRD). This work builds on previous studies, such as, Austin et al. (2004),  
86 Brendryen et al. (2010), Abbott et al. (2011, 2013, 2014, 2016), Davies et al. (2014) and  
87 Griggs et al. (2014), who used similar indicators to assess visible or cryptotephra deposits  
88 within single core sequences.

89

90 We advance that work, with a focus on the time-period between 25-60 ka BP in the North  
91 Atlantic, and define several key types of tephra deposit that share characteristics which are  
92 interpreted as being indicative of common transport, depositional and post-depositional  
93 processes. The tephra deposit types provide a basis for assessing the dominant controls on  
94 tephra deposition in different areas and time periods. Given the wide core network employed  
95 in this study we pinpoint sectors of the North Atlantic Ocean that preferentially preserve  
96 isochronous deposits and these underpin a marine tephra framework presented in Abbott et al.  
97 (submitted). These horizons are the most valuable for establishing independent high-precision  
98 correlations to the Greenland ice-core records to assess the relative timing of abrupt climate  
99 changes.

100

101 **2. Methodology**

102

103 *2.1 Core Network*

104

105 Thirteen marine sequences are included in our core network and each record was investigated  
106 using the same methodological approach (Figures 2 and 3; Table 1). Cores with well-  
107 developed proxy records were prioritised due to the overarching goal of assessing the relative  
108 timing of abrupt climate changes during the last glacial period. In addition, cores from areas  
109 with high sedimentation rates and sufficient material for contiguous tephra sampling were  
110 selected. Overall the network has a wide geographical spread, however, in some instances  
111 paired cores from nearby locations were investigated to assess the stratigraphic integrity of  
112 individual tephra deposits. It was not always possible to fulfil all of these requirements. For  
113 instance, contiguous samples were not available from MD95-2024 and a couple of sites,  
114 M23485-1 and GIK23415-9, do not have well-resolved records of abrupt climate changes.  
115 These sites were included, however, to increase the geographical extent and capture a wide  
116 range of depositional settings.

117

118 *2.2 Identification of Cryptotephra Deposits*

119

120 Cryptotephras were identified and characterised according to the methodological protocol  
121 outlined in Figure 3. Although most aspects of this marine-focussed methodological approach  
122 have been described separately in previous studies, here we synthesise the full procedure.  
123 Core sequences were initially analysed at a low-resolution (5 or 10 cm) using contiguous  
124 samples, i.e. samples taken along the whole length of depth intervals with no gaps between  
125 samples, to provide an initial quantified assessment of tephra content for the whole period of

126 interest. Selected intervals were then reanalysed at a high-resolution (1 cm) depending on a  
127 range of factors, outlined in Section 3, consistent with other studies of both marine and  
128 terrestrial sequences (e.g. Pilcher and Hall, 1992; Lane et al., 2015; Matthews et al., 2015).  
129 Both low and high-resolution samples were processed according to the workflow outlined in  
130 Figure 3.

131

132 Within the protocol, samples are sieved to isolate glass tephra shards in three recommended  
133 size fractions ( $>125\ \mu\text{m}$ ,  $80\text{-}125\ \mu\text{m}$  and  $25\text{-}80\ \mu\text{m}$ ). This is a development of prior studies  
134 that focused on coarser grain size fractions (e.g.  $>150\ \mu\text{m}$  - Austin et al., 2004, Voelker and  
135 Hafliðason, 2015;  $63\text{-}125\ \mu\text{m}$  and  $125\text{-}150\ \mu\text{m}$  – Brendryen et al., 2010), most typically  
136 utilised in the identification of foraminifera, and was driven by the increased identification of  
137 cryptotephra as fine-grained deposits in distal sequences (Davies, 2015). The smallest grain-  
138 size fraction ( $25\text{-}80\ \mu\text{m}$ ) was split using heavy liquid separation into density fractions most  
139 likely to contain glass shards, a procedure initially developed to identify cryptotephra in  
140 terrestrial sediments (Turney, 1998; Blockley et al., 2005). Magnetic separation is an  
141 additional step utilised to separate paramagnetic basaltic material from minerogenic material  
142 with a similar high density ( $>2.5\text{g}/\text{cm}^3$ ; Griggs et al., 2014). Whilst this technique is  
143 infrequently employed for terrestrial sequences, e.g. Mackie et al. (2002), it is routinely  
144 applied in this investigation to aid the isolation and identification of basaltic material. The  
145 high number and proportion of basaltic horizons, relative to rhyolitic horizons, identified in  
146 this study demonstrates the value of including this technique within marine cryptotephra  
147 studies in the North Atlantic. During low-resolution analysis magnetic separation was only  
148 utilised on the  $25\text{-}80\ \mu\text{m}$  size fraction, because the time required for this process was longer  
149 than the time required to count shards from an unseparated sample of the larger fractions.  
150 However, during preparation of samples for geochemical analysis these larger fractions were

151 magnetically separated alongside the 25-80  $\mu\text{m}$  fraction to provide a purer basaltic glass  
152 sample.

153

154 If a low-resolution tephrostratigraphy was being constructed all fractions were inspected for  
155 tephra content using optical microscopy (i.e.  $>125 \mu\text{m}$ ,  $80-125 \mu\text{m}$ ,  $2.3-2.5 \text{ g/cm}^3$  and the  
156  $>2.5 \text{ g/cm}^3$  magnetic fraction; step 12). However, when tephra concentration profiles were  
157 refined at a higher 1 cm resolution some fractions were not inspected. For example, if no  
158 rhyolitic material was present at a low resolution the  $2.3-2.5 \text{ g/cm}^3$  fraction was not  
159 inspected.

160

161 Depending on the nature of the samples and the tephra contained within a sequence,  
162 alternative or additional steps were occasionally adopted (Figure 3). For instance, in some  
163 cores sediment clusters, that appear to consist of sediment bound together by biogenic silica,  
164 were observed (see also Ponomareva et al., in press). These clusters were broken down using  
165 a weak treatment of sodium hydroxide (NaOH) (step 5). This chemical treatment could also  
166 be undertaken after step 3 if clusters are known to be present following initial investigations.  
167 In such a case, the HCl should be washed out of the sediments, but no re-sieving is necessary.  
168 NaOH has previously been used in cryptotephra studies to remove biogenic silicates (e.g.  
169 Rose et al., 1996), with samples warmed to  $90^\circ\text{C}$  for 4 hours, however, it was found that  
170 treatment at room temperature for 1 hr was sufficient to disaggregate the sediment clusters in  
171 this study. As a precaution NaOH treatment was avoided when samples were being prepared  
172 for geochemical analysis, as it has been suggested that NaOH could cause geochemical  
173 modification (e.g. Blockley et al., 2005). However, other studies have shown that such  
174 treatments do not affect the glass composition (e.g. Steinhauser and Bichler, 2008) and

175 experimentation by Ponomareva et al. (in press) indicates that electron-probe micro analysis  
176 (EPMA) analyses are unaffected by this weak NaOH treatment.

177

178 To quantify exceptionally high shard concentrations ( $\sim > 10,000$  per 0.5 g dry weight sediment  
179 (dws)) samples were spiked with Lycopodium spore tablets containing a known quantity of  
180 pollen grains (step 10). The ratio between glass shards and pollen grains is then used to  
181 quantify shard concentrations (e.g. Griggs et al., 2014). This is an adaption of a standard  
182 pollen counting approach previously applied to tephra studies by Gehrels et al. (2006).  
183 Typically, it is not known if this quantification approach is required until low-resolution  
184 analysis has been conducted. As such, if high shard concentrations were observed in low-  
185 resolution samples and it became apparent that shard concentrations would exceed 10,000  
186 shards, counting was halted and the additional step of spiking samples was incorporated into  
187 high resolution analysis of those sections.

188

### 189 *2.3 Geochemical Analysis of Cryptotephra Deposits*

190

191 Shard concentration profiles are employed to select samples for geochemical analysis using  
192 the criteria outlined in Section 3. Samples were re-processed using steps 1-9 of the procedure,  
193 however, the fractions of interest were then mounted in epoxy resin on  $28 \times 48$  mm  
194 microprobe slides to permit thin section preparation (Figure 3). When high shard  
195 concentrations were present all material from the fraction was mounted directly on to the  
196 slides. When tephra was only present at a low concentration ( $\sim < 50$  per 0.5 g dws) glass  
197 shards were picked onto a microprobe slide using a micromanipulator. Shards prepared by  
198 this method are easier to locate during sectioning and EPMA analysis. Flat and polished thin

199 sections of the individual glass shards were produced for EPMA analysis using decreasing  
200 grades of silicon carbide paper and 9, 6 and 1  $\mu\text{m}$  diamond suspension.

201

202 EPMA was conducted at the Tephra Analytical Unit, University of Edinburgh using a  
203 Cameca SX100 with five wavelength dispersive spectrometers over a number of analytical  
204 periods. All shards were analysed using the same operating conditions outlined in Hayward  
205 (2012). Pure metals, synthetic oxides and silicate standards were used for calibration. The  
206 secondary standards of Cannetto Lami Lava, Lipari and BCR2g were analysed at regular  
207 intervals to monitor for instrumental drift within analytical sessions, to assess the precision  
208 and accuracy of analysed samples and to provide a cross-check of the comparability of  
209 analyses between analytical periods. A large number of shards (~20-40 individual shards)  
210 were analysed for each deposit to provide comprehensive characterisations that underpin the  
211 assessment of taphonomic processes, depositional controls and the isochronous nature of  
212 deposits. For all analysis and data comparison the major element data were normalised to an  
213 anhydrous basis, i.e. 100 % total oxides, however, the raw geochemical data utilised here are  
214 provided in the Supplementary Data alongside secondary standard analyses.

215

### 216 ***3. Constructing a Tephrostratigraphy***

217

218 The two major indicators that we employ to assess the integrity of marine tephra deposits are  
219 (i) contiguous high-resolution shard concentration profiles and (ii) rigorous geochemical  
220 characterisation of the glass tephra shards. These are the key aspects of the  
221 tephrostratigraphies defined in this work. Constructing a tephrostratigraphy, however,  
222 involves a series of selections and we illustrate our approach, which aimed for consistency  
223 and comparability between cores, with reference to the record of brown (basaltic) shards in

224 the MD99-2251 core from the Iceland Basin between 1650-1950 cm depth (Figure 4). There  
225 was a distinct lack of colourless shards in this core section but a slight increase was observed  
226 towards the base, which can be related to reworking and redistribution of the underlying  
227 North Atlantic Ash Zone II (NAAZ) II (see Section 4).

228

229 First a low-resolution shard concentration profile is constructed to determine the overall  
230 presence of tephra and to define the background level of glass shards within a sequence (e.g.  
231 Figure 4a). All notable shard peaks were then re-analysed at a high-resolution (1 cm) to refine  
232 their stratigraphic position. This step is crucial as the peak in concentration is typically  
233 thought to represent the timing of atmospheric fallout from a volcanic event (e.g. Ruddiman  
234 and Glover, 1972; Jennings et al., 2002; Davies et al., 2012). Theoretically it is possible for  
235 the maximum shard concentration peak to lie below the original depth of deposition, based on  
236 an interplay of the extent of mixing within and depth of the mixing layer and the  
237 sedimentation rate at the site, however, the impact of this has been assessed as negligible in  
238 practice (Berger and Heath, 1968; Ruddiman and Glover, 1972). Indeed, our focus on high  
239 sedimentation rate sites would negate this effect, however, it is recommended that this is  
240 considered for individual horizons if they are to be used as isochronous tie-lines between  
241 sequences.

242

243 Selecting which peaks to refine at a 1 cm resolution depends on the peak versus background  
244 concentrations, the shape and discreteness of peaks and replication across grain-size fractions  
245 (e.g. Figure 4a). To some extent there is subjectivity in the selection of peaks and no  
246 consistent concentration thresholds could be defined due to variability in peak and  
247 background shard concentrations both within and between the core sequences. In most  
248 instances, but not exclusively, shard concentrations in the 25-80  $\mu\text{m}$  fraction displayed the

249 greatest variability and presence within the records and were the prime criteria for these  
250 selections (e.g. Figure 4a). For some cores, high-resolution investigations were extended over  
251 intervals wider than the main peaks to provide a greater constraint on shard concentration  
252 variations (e.g. between 1678-1698 cm in MD99-2251; Figure 4a) and/or additional samples  
253 were analysed to determine if smaller peaks were due to increased input of material from a  
254 volcanic event or general fluctuations in background shard concentrations (e.g. between  
255 1869-1874 cm and 1879-1884 cm in MD99-2251; Figure 4a). In addition, the time required  
256 for processing and analysing the number of selected samples was considered.

257

258 Reanalysing selected sections at a high-resolution allows an integrated shard concentration  
259 profile to be constructed (e.g. Figure 4b) that, in general, constrains the shard peaks to 1 or 2  
260 cm and higher concentrations were normally observed in the high-resolution counts (e.g.  
261 peaks at 1680-1681 cm and 1904-1905 cm depth in MD99-2251; Figure 4b). This  
262 observation was anticipated, as the low-resolution counts should provide an average of the  
263 tephra concentration over the sampling interval, and has been observed for other cores within  
264 the network. However, there are some examples where lower peak concentrations or very few  
265 shards were observed in the high-resolution samples (e.g. the 1869-1874 and 1879-1884 cm  
266 sections in MD99-2251; Figure 4b). This may be due to uneven lateral distribution of tephra  
267 shards within core sequences, a lack of horizontal continuity and tephra shards being  
268 constrained in pods or lenses. Tephra distributions of this nature have been observed in thin  
269 section (2D) and X-ray microtomography (3D) analysis of North Atlantic marine tephra  
270 sediments (Griggs et al., 2014, 2015). These additional methods can provide further  
271 sedimentological information to aid isochron placement and the interpretation of post-  
272 depositional processes, however, at present they have not been widely applied to tephra  
273 deposits in our network.



274

275 Once an integrated tephrostratigraphy is defined shard peaks are selected for geochemical  
276 analysis to allow the assessment of volcanic source and deposit integrity. Peaks were selected  
277 using criteria akin to those used to pinpoint samples for high-resolution analysis, i.e.,  
278 discreteness relative to background concentrations, replication across grain-size fractions and  
279 processing and analysis time (e.g. Figure 4b).

280

## 281 **4. Results**

282

### 283 *4.1 Classification of individual tephra deposits*

284

285 We applied the same approach to construct a tephrostratigraphic record for all cores within  
286 our network and tephra deposits were identified in the vast majority of records. Tephra shard  
287 concentration profiles, geochemical characterisations and other indicators, such as shard size  
288 and co-variance with IRD, were integrated for these tephra deposits to define a deposit type  
289 classification scheme (Table 2). Five deposit types that share similar physical characteristics  
290 reflecting common modes of delivery and post-depositional reworking are identified (Table  
291 2). This classification scheme is mainly based on deposits of brown glass shards (i.e. basaltic  
292 material) due to the relative lack of colourless shard deposits. However, Type 3, is an  
293 exception and is based on deposits that are most commonly associated with colourless shards  
294 related to NAAZ II, the most widespread silicic tephra found within our core network.

295

296 Deposit Types 1,2 and 3 are all characterised by distinct concentration peaks, however, their  
297 profiles vary in form, displaying discrete (e.g. Figure 5ai), bell-shaped (e.g. Figure 6ai) and  
298 asymmetric (e.g. Figure 7ai) forms respectively, and in spread ranging from 1 cm to up to

299 100 cm (Table 2). These contrasting features are attributed to variable shard concentrations  
300 between the deposit types and differential influence of post-depositional reworking. For  
301 instance, the low shard concentrations in Type 1 deposits contributes towards their  
302 discreteness. Whilst this may result from limited post-depositional reworking, it is also  
303 possible that the low concentration of tephra deposited at the sea-bed is not an adequate tracer  
304 of such activity. Reworking such as bioturbation, however, would most likely not impact the  
305 isochron position (see Section 3). In contrast, the higher input concentrations associated with  
306 Type 2 deposits allows the tephra shards to act as a tracer for bioturbation (e.g. Ruddiman  
307 and Glover, 1972; Griggs et al., 2015), which creates the upward and downward tails in  
308 deposition and roughly bell-shaped profile. This has often been viewed as the classic form of  
309 tephra deposits preserved in marine records (e.g. Ruddiman and Glover, 1972).

310

311 For Type 3 deposits the extremely high shard concentrations rapidly isolated underlying  
312 sediment from bioturbative activity and restricted downward migration of shards, as observed  
313 for the FMAZ II deposit in Griggs et al. (2015). The upward tail and continued deposition of  
314 tephra is primarily attributed to secondary deposition of glass shards from the same volcanic  
315 event from the surrounding sea-bed due to bottom current transportation. Bioturbative  
316 reworking may have also contributed towards increasing the overall spread of these deposits.  
317 In combination these two factors create the observed asymmetric profile (e.g. Figure 7ai;  
318 Table 2). Additional samples in the overall declining concentration profile of Type 3 deposits  
319 were sometimes analysed, particularly when subsidiary peaks were observed, in case any  
320 subsequent volcanic events were obscured within the upward tail. In all instances these  
321 additional analyses had an identical composition to shards in the main peak, corroborating the  
322 assertion that the upward tail was formed mainly through reworking of material from a single  
323 eruption (e.g. Figure 7ai).

324  
325  
326  
327  
328  
329  
330  
331  
332  
333  
334  
335  
336  
337  
338  
339  
340  
341  
342  
343  
344  
345  
346  
347  
348

Deposit Types 1,2 and 3 are most likely derived from single depositional events, yet their isochronous nature can only be fully determined by assessing the relative homo/heterogeneity of their geochemical signature. Type 1 and 3 deposits have a homogenous signature, i.e. all analysed shards form a single geochemical population most likely sourced from one volcanic eruption, which strongly suggest that they were deposited via primary airfall and are useful isochronous tephra markers (e.g. Figure 5aii for Type 1 deposits and Figure 7ai for a Type 3 deposit). Type 2 deposits are sub-divided into Type 2A, which have a homogenous composition, and Type 2B, which have a heterogenous composition, i.e. the analysed shards form multiple populations and/or reveal a widespread of analyses with high variability and limited consistency. Figures 6a and 6b provide examples of homogeneity for two Type 2A deposits, whilst, Figure 5b provides examples of the heterogeneity observed for two Type 2B deposits. This sub-categorisation is important as the homogenous Type 2A deposits are likely to be isochronous, akin to Type 1 and 3 deposits, while the heterogeneity of Type 2B deposits most likely reflects the deposition of products from multiple eruptions and probably secondary transport processes that affect the isochronous nature of the horizons. For example, geochemical heterogeneity is a key indicator of transport via iceberg rafting and the amalgamation of the products of closely timed eruptions (Griggs et al., 2014). An additional line of evidence for Type 2B deposits is co-variance of shard concentrations with IRD records. The relative proportion of shards across the different grain-size fractions can also help determine transport processes as sea-ice rafting typically transports shards larger than would be expected via primary airfall to distal sites (e.g. Austin et al., 2004). Overall, for Type 2 deposits a careful assessment of a range of key indicators is required to determine their value as isochronous deposits.

349 In contrast, to the single concentration peaks displayed by deposit Types 1,2 and 3, Type 4  
350 deposits display multiple peaks over a period of elevated shard concentrations whereas Type  
351 5 deposits are characterised by tephra in multiple consecutive samples, but no clear pattern or  
352 peaks in shard concentrations (Table 2). In most cases, the multiple peaks seen in the Type 4  
353 deposits display heterogeneous compositions but typically a common geochemical signature,  
354 e.g. the wide 456-473 cm depth deposit in MD04-2820CQ (Figure 7b; Abbott et al., 2016).  
355 This indicates that the entire deposit is an amalgamation of eruptive material from several,  
356 closely timed, volcanic eruptions and that the multiple peaks are the product of secondary  
357 transport processes (e.g. bioturbation and bottom current reworking) rather than primary  
358 airfall. Alternatively, the glass shards found in Type 4 deposits may have been amalgamated  
359 during deposition on the Icelandic ice-sheet and subsequently transported to core sites via  
360 iceberg rafting. As with Type 2B deposits, further insights into the mode of deposition may  
361 be gained by comparing shard concentration profiles with iceberg rafting proxies. Without a  
362 distinct concentration peak or geochemical evidence that they were sourced from a single  
363 eruption Type 4 deposits typically cannot be utilised as isochronous marker horizons for  
364 high-precision correlations. However, they have the potential to be used as regional marine-  
365 marine core tie-lines, as suggested for FMAZ III by Abbott et al. (2016).

366

367 Type 5 deposits are commonly identified during low-resolution investigations. Only selected  
368 deposits were re-evaluated at a high-resolution and for geochemical composition. No distinct  
369 concentration peaks were identified, and geochemical analyses revealed heterogeneous  
370 populations of shards that were geochemically identical to underlying deposits, e.g. NAAZ II.  
371 As such, Type 5 deposits are interpreted as a background of glass shards that are deposited at  
372 the core sites and dispersed in the sediment column by remobilisation and reworking  
373 processes. These background signals vary between sites and may mask and hamper the

374 identification of primary airfall events that only deposited a low concentration of glass  
375 shards. High-resolution analysis coupled with intensive geochemical characterisation may  
376 isolate such events and would be appropriate if specific volcanic events were being targeted,  
377 however, this was not feasible within our extensive core network.

378

#### 379 *4.2 Categorising core sequences using the tephra classification scheme*

380

381 The tephra classification scheme has been employed to categorise the cores according to the  
382 presence and dominance of different deposit types. Four core categories have been identified  
383 (Figure 8) and range from sites dominated by primary airfall deposits (green sites) to sites  
384 with deposits affected by secondary processes (red sites). In addition, very few shards were  
385 identified in the northernmost (JM04-25PC from the Western Svalbard slope) and  
386 southernmost (MD01-2444 from the Iberian Margin) records. Trace amounts (1-2 shards)  
387 were identified in some low-resolution samples but none were replicated as significant  
388 deposits during high-resolution analysis.

389

##### 390 *4.2.1 Core dominated by Type 1 deposits*

391

392 Only two marine sequences exclusively contain Type 1 deposits, MD04-2822 from the  
393 Rockall Trough and MD04-2829CQ from the Rosemary Bank (Figure 8). The Type 1  
394 deposits are discrete peaks in brown shard concentrations constrained within ~1 cm and both  
395 sites have a limited background of brown shards over the period of interest (e.g. Figure 5ai).  
396 Shards from the discrete peaks have single homogenous geochemical populations that can be  
397 directly related to single volcanic source regions (Figure 5aai) and as such are thought to  
398 represent isochronous marker horizons. The shard concentrations were low (~5-40 shards per

399 0.5 g dws in the 25-80  $\mu\text{m}$  fraction) and occasionally replicating these peaks to extract shards  
400 for geochemical analysis was challenging. This may be a consequence of the uneven  
401 distribution of shards within the cores, however, the successful identification of these Type 1  
402 deposits does demonstrate how the approach adopted in this work can be used to trace such  
403 low concentration deposits.

404

#### 405 *4.2.2 Cores containing Single Type 2A Deposits*

406

407 Two cores, MD95-2010, from the Norwegian Sea, and MD01-2461, from the Porcupine  
408 Seabight, each contain just one significant tephra deposit with bell-shaped shard  
409 concentration profiles (Figure 6ai and bi). These deposits were identified because a  
410 significant number of shards were isolated over 10-20 cm intervals in the low-resolution  
411 counts. Given their homogenous geochemical compositions, these are both classified as Type  
412 2A deposits (Figure 6aii and bii) and are thought to be isochronous markers. Evidence of  
413 upward reworking within MD01-2461 is seen by a small subsidiary tephra shard peak  
414 positioned 4-5 cm above the highest shard concentrations with an identical geochemical  
415 composition at both depths (Figure 6b). In both cores only trace amounts (<2-3) of shards  
416 were present in the rest of the low-resolution samples, apart from ~10 shards identified  
417 around NAAZ II in MD95-2010.

418

#### 419 *4.2.3 Cores containing Mixed Deposit Types*

420

421 Five of the core sites have been grouped into this category (Figure 8) and contain a range of  
422 deposit types. Type 2 deposits dominate and these are typically relatively discrete with high  
423 shard concentrations, however the geochemical compositions range between homogenous

424 (Type 2A) and heterogenous (Type 2B). Type 4 deposits are also present in some sequences  
425 and at most sites the rhyolitic component of NAAZ II is present as a Type 3 deposit. The  
426 MD04-2820CQ record is a prime example of this category. It contains a number of Type 2  
427 deposits, with differing geochemical homogeneity, the FMAZ III as a Type 4 deposit and the  
428 NAAZ II rhyolitic component as a Type 3 deposit (Abbott et al., 2016). The variability in  
429 tephra deposit types means that a careful assessment of deposits is required and strongly  
430 suggests that the depositional controls at these sites varied temporally throughout the last  
431 glacial period.

432

#### 433 *4.2.4 Core dominated by Type 2B and Type 4 deposits*

434

435 Two cores have been grouped within this category, SU90-24 from the Irminger Basin and  
436 M23485-1 from the Iceland Sea (Figure 8). These sites are characterised by multiple  
437 concentration peaks within a high background level of shards, e.g. 1,000-10,000s of shards  
438 per 0.5 g dws. Peaks in shard concentration are not well-resolved in these records and the  
439 distinct contrast between SU90-24 and a Type 1 dominated core (MD04-2822) is shown in  
440 Figure 5. For SU90-24, single-shard analyses from some of the concentration peaks have  
441 highly heterogenous geochemical signatures, with a wide range of major oxide values that  
442 span several different Icelandic volcanic systems (Figure 5b). Given the shard concentration  
443 profiles and compositional results, these deposits are classified as Type 2B and Type 4.  
444 M23485-1 is dominated by Type 4 deposits with two major depositional pulses of  
445 heterogenous basaltic and rhyolitic material. Overall, the deposits found in these cores cannot  
446 be considered as isochronous horizons.

447

### 448 ***5. Discussion - Controls on Ash Deposition and Preservation***

449

450 The core categorisation highlights that a diverse range of tephrostratigraphies were preserved  
451 during the last glacial period across the North Atlantic. Geographical clustering of similar  
452 core sites suggests that there were both spatial and temporal controls on ash deposition.

453 Various factors could have controlled the transport and deposition of tephra, including (i) the  
454 nature of volcanism inputting tephra into the system, (ii) atmospheric dispersal patterns and  
455 distance from eruptive source, (iii) rafting by icebergs and sea-ice and (iv) the rate and nature  
456 of sedimentation. Local factors may have also operated at individual cores sites. Through an  
457 assessment of these factors we propose that for our core categories we identify common  
458 controls operating within different sectors of the North Atlantic (Figure 9).

459

#### 460 *5.1 Frequency and Composition of Icelandic Volcanism*

461

462 The marine tephra records are ultimately controlled by the nature and frequency of Icelandic  
463 eruptions as this provides the primary input of tephra into the North Atlantic. Currently the  
464 most well-resolved record of Icelandic eruptions during the glacial period is derived from the  
465 Greenland ice-cores (Bourne et al., 2015) as proximal records are relatively limited due to the  
466 removal of material by glacial activity and the burial of deposits by subsequent volcanic  
467 activity. Within the Greenland ice-cores over 99 tephra deposits have been identified in this  
468 time period, which is significantly higher than the number identified within our marine tephra  
469 framework, but could suggest that some of the marine deposits have amalgamated material  
470 from multiple eruptions (e.g. FMAZ III in JM11-19PC and MD04-2820CQ; see Figure 7b).  
471 Within our core network there is a greater abundance of basaltic horizons in comparison to  
472 rhyolitic deposits, which is consistent with the Greenland ice-core records, as 95 % of these  
473 deposits are basaltic (Bourne et al., 2015). This dominance of far-travelled basaltic material



474 within distal sites could be due to the increased ice cover during the last glacial period which  
475 implies that the horizons were derived from subglacial phreatomagmatic eruptions, which can  
476 enhance the explosivity of basaltic eruptions due to the presence of water (Larsen and  
477 Eiriksson, 2008). The relative lack of rhyolitic horizons in the ice-cores suggests that the  
478 rhyolitic background of shards observed in many of the marine records is most likely due to  
479 reworking of material from NAAZ II, rather than resulting from subsequent volcanic activity.

480

### 481 *5.2 Atmospheric Dispersal Patterns and Proximity to Iceland*

482

483 Following a volcanic eruption the wind-driven dispersal patterns will dictate the location of  
484 airfall deposition. The proximity of a core site to the volcano is important as the grain-size,  
485 shard concentration and thickness of airfall deposits decreases exponentially away from the  
486 eruptive source. Atmospheric transport skews this relationship with extended transport of  
487 material along transport axes downwind from the eruptive source and this bias is more  
488 evident at distal sites (Sparks et al., 1981; Pyle, 1989; Lacasse, 2001).

489

490 The four cores solely preserving deposits thought to be transported via primary airfall (i.e.  
491 green and orange sites containing Type 1 and Type 2A deposits: MD95-2010, MD04-  
492 2829CQ, MD04-2822 and MD01-2461) are located between the south and east of Iceland, in  
493 an oceanic sector stretching from the south coast of Ireland to the west coast of Norway, with  
494 the two green sites containing multiple deposits lying close together towards the SE off the  
495 west coast of Scotland (Figure 9). Other sites that preserve a mix of deposit types including  
496 some deposited via atmospheric transport, i.e. yellow coded sites, also generally lie to the  
497 south and east of Iceland with the exception of MD95-2024 (Figure 9). This clustering of

498 sites suggests that tephra was transported from Iceland via westerly winds, consistent with  
499 dominant wind patterns and the nature of Icelandic eruptions.

500

501 Modern observations indicate that wind direction changes progressively with altitude in the  
502 troposphere, with easterlies dominating at ground level shifting to southerly at a low level  
503 (1.4 km) and westerlies in the upper troposphere and lower stratosphere between 9-15 km  
504 throughout the year (Lacasse, 2001). Above 15 km altitude seasonal variability is observed  
505 with strong westerlies during the autumn and winter and relatively weak easterlies during the  
506 spring and summer (Lacasse, 2001). The modern atmospheric patterns are utilised as an  
507 analogue for dispersal of tephra during the glacial period as the reconstruction of glacial wind  
508 patterns is complex. Studies do suggest, however, that surface circulation was more intense  
509 over the North Atlantic during the last glacial period (e.g. Mayewski et al., 1994; Kutzbach  
510 and Wright, 1985). Plume heights from modern basaltic eruptions similar in nature to those  
511 that occurred during the last glacial period (e.g. Vatnajökull 1996, Hekla 2000, Grímsvötn  
512 2004 and 2011 and Eyjafjallajökull 2010) were typically between ~8-15 km with some  
513 reaching 25 km altitude (Gudmundsson et al., 2004; Höskuldsson et al., 2007; Kaminski et  
514 al., 2011; Oddsson et al., 2012; Petersen et al., 2012). For older eruptions, Lacasse (2001)  
515 deduced from proximal and distal grain sizes that the Saksunarvatn Ash, erupted from  
516 Grímsvötn in the early Holocene, produced an eruption column of at least 15 km. Eruptive  
517 plume heights together with dominant wind directions suggest that basaltic tephra was mainly  
518 atmospherically transported away from Iceland in an easterly direction and is consistent with  
519 our findings.

520

521 Southward atmospheric dispersal of some tephtras, to core sites such as MD99-2251 and  
522 MD04-2820CQ, may be a consequence of modification by more variable surface wind

523 conditions that reflect the weather at the time of an eruption (Lacasse, 2001). A similar  
524 scenario was observed for the Eyjafjallajökull 2010 eruption, with weather conditions  
525 exerting a strong influence following initial easterly transport of tephra (Davies et al., 2010).  
526 Other variable influences such as precipitation, the timing of the eruption, style of volcanism,  
527 magma discharge rate and height of eruptive column may have also created differences from  
528 the general pattern for individual eruptions. Although our observations indicate dispersal  
529 towards the south, no tephra deposits were preserved in the southernmost site MD01-2444,  
530 most likely due to the long distance between this site and the main Icelandic source.

531

532 Preferential atmospheric transport of ash to the east and south of Iceland is also consistent  
533 with the identification of airfall tephra horizons from Iceland in terrestrial deposits from sites  
534 in NW Europe (e.g. Lawson et al., 2012) and their absence to the west and southwest of  
535 Iceland (e.g. Greenland – Blockley et al., 2015; eastern North America - Pyne-O'Donnell et  
536 al., 2012; Mackay et al., 2016). Tephra is preserved at the most westerly site, MD95-2024.  
537 This core is downwind and the second furthest from Iceland with greater peak and  
538 background shard concentrations relative to closer downwind sites such as MD04-2829CQ  
539 and MD04-2822. This conflicts with the expected atmospheric dispersal pattern of tephra and  
540 proximity to source, strongly indicating that other processes were controlling tephra delivery  
541 to the North Atlantic west of Iceland.

542

543 The observation of limited atmospheric dispersal in a northerly direction from Iceland has  
544 some conflicts with the observations of Bourne et al. (2015) who inferred direct transport of  
545 ash in a north westerly direction to the Greenland ice-sheet (Figure 9). However, this could  
546 be a consequence of marine sites north of Iceland being more dominantly influenced by other  
547 controls, such as ice-rafting deposition of tephra (see discussion below), which masked any

548 isochronous deposits. The distance from source was highly likely to be a dominant control on  
549 the non-preservation of tephra at the most northerly site JM04-25PC.

550

551 Overall, therefore, while atmospheric transport was the primary mechanism delivering tephra  
552 to the green and orange sites it was only a partial control on the delivery of tephra to the  
553 yellow sites. At those locations other controls had an additional influence, leading to the  
554 identification of some non-isochronous deposits.

555

### 556 *5.3 Ice-Rafting of Tephra and Ocean Currents*

557

558 The potential for tephra to have been rafted either by sea-ice or icebergs prior to deposition in  
559 the glacial North Atlantic has been highlighted previously and this process can transport  
560 material along different trajectories and further from the source than atmospheric dispersal.

561 Three distinct areas that preserve tephra deposited by rafting processes, i.e. Deposit Types 2B  
562 and 4, have been identified. These areas are the Iceland Sea and Irminger Basin to the north  
563 and west of Iceland (core sites M23485-1 and SU90-24), the mid Atlantic (MD95-2024,  
564 MD99-2251, GIK23415-9, MD04-2820CQ) and NE of the Faroe Islands (JM11-19PC).

565 Whilst the Iceland Sea and Irminger Basin were heavily influenced by these processes  
566 throughout the 25-60 ka BP period, both Type 2A and Type 2B deposits were preserved in  
567 the other two areas suggesting that the influence of rafting was temporally variable (Figure  
568 8).

569

570 Surface ocean currents have a huge role to play in the trajectory of tephra-bearing sea-ice and  
571 icebergs away from Iceland (Bigg et al., 1996) and thus the deposition of tephra at core sites  
572 during melting. Modern surface ocean currents are illustrated on Figure 9 and are used as an

573 analogue for the glacial period. The North Atlantic Drift (NAD) from the SW dominates the  
574 warm surface ocean currents and splits into the Irminger Current south of Greenland and the  
575 North Iceland Irminger Current around Iceland before flowing into the Nordic Seas. Cold  
576 currents are dominated by the East Greenland Current flowing down the east coast of  
577 Greenland. A distinct feature of the surface circulation is the subpolar gyre, an anti-clockwise  
578 ocean surface circulation south of Iceland (Figure 9). These surface ocean currents would  
579 have strongly influenced ice-rafting but the source of icebergs and sea-ice extent was also an  
580 important factor.

581

582 The expanded size of the LGM ice-sheet over Iceland suggests that ice calving margins could  
583 have been located all around the island (Figure 9). With the majority of the major volcanic  
584 centres located in the south of the island, icebergs from the southward margin may have  
585 contained a greater concentration of tephra, however, local atmospheric transport north, east  
586 and west of the volcanoes would have contributed material to icebergs calving from all of  
587 these margins. The surface circulation patterns shown in Figure 9 suggests that icebergs from  
588 all margins could have been transported in surface ocean currents. Sea-ice reconstructions  
589 have shown that its extent over the North Atlantic region varied in time with the DO and  
590 Heinrich events (Hoff et al., 2016). It has been suggested that sea-ice retreated abruptly  
591 during the warming at the start of interstadials, but spread rapidly from the coast of  
592 Greenland during interstadial cooling with perennial sea-ice extending beyond Iceland during  
593 cold stadials and reaching a greater extent during Heinrich events (Figure 9; Hoff et al.,  
594 2016). This temporal variability in sea-ice coverage and its rafting along similar trajectories  
595 to those proposed for icebergs is likely to have played a role in the dispersal of tephra.

596

597 Iceberg rafting from the north coast of Iceland was the likely primary control on tephra  
598 deposition north and west of Iceland. The M23485-1 site lies close to the northern margin of  
599 the LGM Icelandic ice sheet and icebergs calved from this margin could have been entrained  
600 within the East Greenland Current and deposited material over the SU90-24 site. In addition,  
601 sea-ice rafting may have contributed towards this pattern of tephra deposition as the latter site  
602 lies within the stadial perennial ice-sheet limits and would have been covered early in the  
603 advances during interstadial cooling phases. Within the mid-Atlantic area Icelandic icebergs  
604 transported in the sub-polar gyre are likely to have deposited material at both the MD95-2024  
605 and MD99-2251 sites. The MD04-2820CQ and GIK23415-9 sites lie within the IRD Belt, an  
606 area of the North Atlantic within which IRD from the Laurentide Ice Sheet was deposited  
607 during Heinrich Events, and may have been influenced by Icelandic icebergs transported in  
608 this zone by surface currents (Figure 9). Indeed, glass shards have been found in association  
609 with the lithic Heinrich layers (e.g. Obrochta et al., 2014). The influence of sea-ice rafting in  
610 the mid-Atlantic would have been temporally variable throughout the glacial period and  
611 should not be ruled out as a potential process for ash transport and deposition as MD95-2024  
612 and MD99-2251 lie close to the stadial perennial sea ice limit and MD04-2820CQ and  
613 GIK23415-9 lie close to the Heinrich event limit (Figure 9). The area to the NE of the Faroe  
614 Islands, the JM11-19PC site, may have been influenced by both rafting processes, with  
615 icebergs transported from the North coast of Iceland in the North Iceland Irminger Current  
616 and it lies close to the limit of perennial sea-ice during stadial periods. For all sites potentially  
617 affected by rafting processes key indicators such as the level of geochemical heterogeneity  
618 and shard sizes should be utilised to assess individual deposits.

619

620 The lack of rafted deposits in the MD04-2822 and MD04-2829CQ cores may be due to the  
621 Rockall Trough, the main pathway by which the warm North Atlantic surface water flows

622 northward into the Norwegian Sea, effectively isolating them from the influence of Icelandic  
623 icebergs. The sites lie close to the stadial perennial sea ice limit so could be susceptible to sea  
624 ice rafting, however, the tephrostratigraphic records strongly indicate that this process has not  
625 deposited tephra at these particular sites. Continuous sea-ice cover can be ruled out as a  
626 potential control on the lack of tephra preservation at the northerly JM04-25PC site. The  
627 reconstructed sea-ice limits from Hoff et al. (2016) suggest that while the site is the most  
628 northerly sea-ice cover was limited to stadial phases and Heinrich events and was not greater  
629 than at other sites, e.g. SU90-24 and M23485-1, containing significant tephra deposits  
630 (Figure 9).

631

#### 632 *5.4 Nature and Rate of Sedimentation*

633

634 Sedimentation rates are a further important a control on tephra preservation. They provide  
635 information on the nature of sedimentation and slower rates of sedimentation increase the  
636 likelihood that the products of separate but closely timed eruptions are amalgamated. Table 1  
637 presents approximate average sedimentation rates for all the sites in the core network  
638 between 25-60 ka BP. In general, all the sites had relatively high sedimentation rates, a bias  
639 created by our prioritisation of sites to include in the network (see Section 2.1).

640

641 These high sedimentation rates may indicate that, in addition to sedimentation occurring  
642 through pelagic settling, bottom currents were also transporting material to the sites (Rebesco  
643 et al., 2014). Thus, the sites incorporated in the network may have an increased susceptibility  
644 to secondary deposition of tephra shards via bottom current reworking. This process could  
645 account for the persistent low background levels of glass shards at most sites (Type 5  
646 deposits) and occasional outlying single shard analyses in the tephra deposits (see Abbott et

647 al., submitted). However, bottom current reworking does not appear to have been a  
648 significant control on the nature of these tephra records. The only deposit type that we  
649 interpret as being formed and affected by this process is Type 3 and this can be attributed to  
650 the exceptionally high peak shard concentrations in comparison to the other deposit types  
651 (Table 2). Almost exclusively Type 3 deposits are associated with NAAZ II, a unique event  
652 that led to the input of a sufficient concentration of shards into the oceanic system to be  
653 reworked and act as a tracer for bottom current activity. As with bioturbation, the lack of  
654 evidence of reworking for other deposits does not definitively demonstrate that this process  
655 was not occurring, because the tephra concentrations could have been too low to act as an  
656 adequate tracer.

657

658 There is no clear difference in sedimentation rates between the cores containing only  
659 isochronous deposits (i.e. green and orange sites) and those dominated by heterogenous  
660 secondary deposits (i.e. red sites) with estimated rates of 14-20 cm/ka and 17-19 cm/ka  
661 respectively (Table 1; Figure 8). However, in general the sites containing a mix of deposit  
662 types (yellow sites; Figure 8) have lower sedimentation rates, between 9-11 cm/ka, apart  
663 from the MD95-2024 site which had a rate of 22 cm/ka (Table 1). This contrast in  
664 sedimentation rates is a general reflection of these cores deriving from the deepest sites in the  
665 network, away from terrestrial sediment sources and the higher sedimentation rates observed  
666 on continental shelves (Figure 9). The low sedimentation rates may have contributed towards  
667 the occurrence of Type 2B and Type 4 deposits at these sites due to the increased likelihood  
668 of eruptive products being amalgamated. With Icelandic basaltic tephra horizons in the  
669 Greenland ice-cores having an average recurrence interval of ~1 per 200 years during this  
670 period (Bourne et al., 2015) and 200 years being represented by ~2 cm depth at the yellow  
671 sites it is highly likely that closely spaced eruptions were mixed. The lower sedimentation



672 rates would also have contributed to slower upward migration of the bioturbation mixing  
673 zone, promoting the amalgamation of deposits and elongation of the shard concentration  
674 profile for Type 2 deposits. Each deposit must be evaluated individually as these sites may  
675 also be heavily influenced by rafting processes, which can produce Type 2B deposits with  
676 geochemical heterogeneity. Overall, the lower sedimentation rates and thus temporal  
677 resolution at all these sites could account for the lower number of tephra horizons identified  
678 within the marine core network in comparison to the Greenland ice-core records (see Abbott  
679 et al., submitted for further discussion).

680

### 681 *5.5 Local Site Conditions*

682

683 Based on their proximity to Iceland, atmospheric dispersal patterns and tephra rafting in the  
684 North Atlantic one might expect MD95-2010 and MD01-2461 to both contain a number of  
685 tephra deposits. Both, however, only contained a single tephra deposit, the FMAZ IV and  
686 NAAZ II respectively, strongly suggesting another factor was limiting the deposition of  
687 tephra at these sites. Both sites lie close to the former limits of LGM ice sheets and are  
688 amongst the shallowest sites in the network (Figure 9; Table 1). Higher levels of terrigenous  
689 sediment deposition might have masked or diluted the tephra records at these sites, especially  
690 if the material was large and/or dense as the tephra concentrations presented in this work are  
691 referenced to overall sediment weight.

692

### 693 *5.6 Summary*

694

695 Overall, whilst only a small area of the North Atlantic was disposed to solely preserving  
696 isochronous Type 1 and Type 2A deposits, these primary deposits can also be preserved in a

697 wide area to the east and south of Iceland due to atmospheric dispersal patterns. Only a small  
698 area to the north and west of Iceland does not preserve any isochronous deposits. We suggest  
699 that the most significant factor complicating the tephrostratigraphic records is the rafting of  
700 tephra within icebergs and sea-ice, which can be constrained spatially but also displays  
701 temporal variability, particularly at sites within the central North Atlantic. In addition, the  
702 high frequency of Icelandic volcanic eruptions during the period provides a constraint on  
703 tephra records as despite our focus on sites with high sedimentation rates they are potentially  
704 still too low to resolve individual events.

705

## 706 ***6. Conclusions***

707

708 This work provides an integrated methodology for the identification of cryptotephra in North  
709 Atlantic marine records alongside a protocol for assessing the integrity of deposits and the  
710 influence of primary and secondary transport and depositional processes. This has been  
711 applied to a widespread network of cores from which five key tephra deposit types with  
712 common physical characteristics and depositional and transport histories have been defined.  
713 These range from valuable airfall deposited isochronous horizons, to geochemically  
714 heterogenous deposits with complex histories, to persistent background signals of ash  
715 deposition. While the variety of deposit types observed in the glacial North Atlantic reflects  
716 the complexity of processes controlling the transport, deposition and post-depositional  
717 reworking of tephra and may be unique to this setting, the methodological approach for  
718 identification could underpin investigations in other oceanic regions.

719

720 A regional analysis of the tephrostratigraphic records has shown that a range of different  
721 controls influenced tephra deposition and the deposit types preserved at different sites within

722 the North Atlantic over the last glacial period. A key area to the southeast of Iceland was  
723 sheltered from any ice-rafting influence and only isochronous airfall deposits have been  
724 isolated in these records. However, primary deposits were also identified in a wide oceanic  
725 sector between the south and east of Iceland, which could be the focus of future studies to  
726 identify further isochronous horizons or to trace those identified within this work. The  
727 significance of the isochronous horizons in this work is discussed in Abbott et al. (submitted),  
728 which defines the framework of marine tephra horizons for the 25-60 ka BP period in the  
729 North Atlantic region.

730

### 731 *Acknowledgements*

732

733 This work was financially supported by the European Research Council (TRACE project)  
734 under the European Union's Seventh Framework Programme (FP7/2007-2013) / ERC grant  
735 agreement no. [259253]. PMA also acknowledges support from the European Research  
736 Council under the European Union's Horizon 2020 research and innovation programme  
737 (grant agreement No 656381). Thanks to William Austin, Henning Bauch, Mark Chapman,  
738 Frederique Eynaud, Ian Hall, Claude Hillaire-Marcel, Elisabeth Michel, Tine Rasmussen,  
739 Bjørg Risebrobakken, James Scourse, Mara Weinelt and the British Ocean Sediment Core  
740 Research Facility (BOSCORF) for providing samples or access to the marine cores utilised  
741 within this study. We would like to thank Dr Chris Hayward for his assistance with the use of  
742 the electron microprobe at the Tephrochronology Analytical Unit, University of Edinburgh.  
743 Thanks also to Gareth James, Gwydion Jones and Kathryn Lacey (Swansea University) for  
744 assistance with laboratory processing. This paper contributes to the EXTRAS project  
745 (EXTending TephRAS as a global geoscientific research tool stratigraphically, spatially,  
746 analytical, and temporally within the Quaternary), an INTAV-led project (International Focus

- 747 Group on Tephrochronology and Volcanism) within the Stratigraphy and Chronology
- 748 Commission (SACCOM) of the International Union for Quaternary research (INQUA).

749 **Figures Captions**

750

751 **Figure 1:** Flow chart of the transportation and depositional processes that could have affected  
752 tephra within the glacial North Atlantic prior to preservation in marine sediments. Adapted  
753 from Griggs et al. (2014).

754

755 **Figure 2:** Network of North Atlantic marine cores studied within this work and ice-cores  
756 mentioned within the text.

757

758 **Figure 3:** Flow chart of the consistent methodology utilised to determine the tephra content  
759 of cores within the marine network and extract and prepare glass shards for geochemical  
760 analysis. NaOH = sodium hydroxide. SPT = sodium polytungstate.

761

762 **Figure 4:** Example of the construction of a tephrostratigraphy using the MD99-2251 core. (a)  
763 Low-resolution brown glass shard concentration profiles split into three grain-size fractions.  
764 Blue bars denote depth intervals reinvestigated at a 1 cm resolution. (b) Integrated high and  
765 low resolution brown shard counts for the MD99-2251 core. Shard counts have been  
766 truncated for clarity. Shard counts in the 1686-1687 cm sample (\*) are 4991, 1862 and 507  
767 shards per 0.5 g dws in the 25-80, 80-125 and >125  $\mu\text{m}$  grain-size fractions respectively. The  
768 shard count for the 25-80  $\mu\text{m}$  grain-size fraction from the 1904-1905 cm sample (\*\*) are  
769 3776 shards per 0.5 g dws. Red bars denote samples depths from which glass shards were  
770 subsequently extracted for compositional characterisation.

771

772 **Figure 5:** Comparison of (i) tephrostratigraphic records and (ii) compositional  
773 characterisations of tephra deposits from the (a) MD04-2822 and (b) SU90-24 marine

774 sequences. Brown shard counts for the 25-80  $\mu\text{m}$  grain-size fraction from 470-500 cm in  
775 SU90-24 have been truncated for clarity. Shard counts exceed 40,000 shards per 0.5 g dws,  
776 however, two peaks could be identified at 480-481 cm and 486-487 cm. Np(s) record for  
777 MD04-2822 from Hibbert et al. (2010). Magnetic susceptibility record for SU90-24 from  
778 Elliot et al. (2001). Geochemical fields for Icelandic volcanic systems from Bourne et al.  
779 (2015) and references within. Within MD04-2822 additional discrete peaks can be observed,  
780 e.g. at 1731-1732 cm and 1965-1966 cm, however, it was not possible to acquire sufficient  
781 material for geochemical characterisation.

782

783 **Figure 6:** Examples of shard concentration profiles and geochemical characterisations for  
784 Type 2A tephra deposits from two North Atlantic marine records within the network. (a)  
785 MD95-2010 (i) 910-920 cm high-resolution tephrostratigraphy of brown glass shards (ii)  
786 compositional variation diagrams of analyses from glass shards extracted from the 915-916  
787 cm depth sample. Chemical classification and nomenclature for total alkalis versus silica plot  
788 after Le Maitre et al. (1989) and division line to separate alkaline and sub-alkaline material  
789 from MacDonald and Katsura (1964). Geochemical fields for Icelandic tholeiitic volcanic  
790 systems defined using whole rock analyses from Jakobsson et al. (2008) (Reykjanes),  
791 Höskuldsson et al. (2006) and Óladóttir et al. (2011) (Kverkfjöll) and Jakobsson (1979),  
792 Haflidason et al. (2000) and Óladóttir et al. (2011) (Grímsvötn and Veidivötn-Bardabunga).  
793 (b) MD01-2461 (i) 940-950 cm high-resolution tephrostratigraphy of colourless glass shards  
794 (ii) total alkalis versus silica plot of analyses from glass shards extracted from the 947-948  
795 cm depth sample. Normalised compositional fields for the Icelandic rock suites derived from  
796 whole rock analyses in Jakobsson et al. (2008).

797

798 **Figure 7:** Examples of shard concentration profiles and geochemical characterisations for a  
799 (a) Type 3 and a (b) Type 4 deposits from two North Atlantic marine records within the  
800 network. (a) MD99-2251 (i) 1950-2030 cm tepthrostratigraphy of colourless glass shards  
801 integrating low and high-resolution shard counts (ii) compositional variation diagrams  
802 comparing characterisations of colourless glass shards from 1974-1979 cm and 2014-2015  
803 cm depth. (b) MD04-2820CQ (i) 450-480 cm high-resolution tepthrostratigraphy of brown  
804 glass shards (ii) compositional variation diagrams comparing characterisations from four  
805 shard peaks within the Type 4 deposit. Data from Abbott et al. (2016). Chemical  
806 classification and nomenclature for total alkalis versus silica plot after Le Maitre et al. (1989)  
807 and division line to separate alkaline and sub-alkaline material from MacDonald and Katsura  
808 (1964).

809

810 **Figure 8:** Classification of core sites within the marine core network. See Section 4.2 for  
811 details of classes.

812

813 **Figure 9:** Primary controls and influences on the deposition of tephra within the glacial  
814 North Atlantic Ocean. Ocean surface currents and names from Voelker and Haflidason  
815 (2015) and Rasmussen et al. (2016). Currents: IC = Irminger Current; NIIC = North Iceland  
816 Irminger Current; EGC = East Greenland Current; EIC = East Iceland Current; NAD = North  
817 Atlantic Drift; SPG = Sub-polar Gyre. Last Glacial Maximum (LGM) ice limits from Dyke et  
818 al. (2002), Funder et al. (2011) and Hughes et al. (2016). Perennial sea ice limits from Hoff et  
819 al. (2016). Core classification from Figure 7.

820

821 **Supplementary Information**

822

823 **Table S1:** Major oxide concentrations of shards from tephra deposits in the MD04-2822 core.  
824 Deposits analysed are from the depths of (i) 1836-1837 cm (ii) 2004-2005 cm and (iii) 2017-  
825 2018 cm.

826

827 **Table S2:** Major oxide concentrations of shards from tephra deposits in the SU90-24 core.  
828 Deposits analysed are from the depths of (i) 340-342 cm (ii) 420-422 cm (iii) 480-481 cm and  
829 (iv) 486-487 cm.

830

831 **Table S3:** Major oxide concentrations of shards from the MD95-2010 915-916 cm tephra  
832 deposit.

833

834 **Table S4:** Major oxide concentrations of shards from MD01-2461 related to the rhyolitic  
835 component of North Atlantic Ash Zone II (II-RHY-1). Deposits analyses are at (i) 942-943  
836 cm and (ii) 2014-2015 cm depth.

837

838 **Table S5:** Major oxide concentrations of shards from MD99-2251 related to the rhyolitic  
839 component of North Atlantic Ash Zone II (II-RHY-1). Deposits analyses are at (i) 1974-1975  
840 cm and (ii) 947-948 cm depth.

841

842 **Table S6a:** Secondary standard analyses of the BCR2g standard made throughout analytical  
843 periods during which sample analyses presented in this work were analysed.

844

845 **Table S6b:** Secondary standard analyses of the Lipari standard made throughout analytical  
846 periods during which sample analyses presented in this work were analysed.

847



848 **References**

849

850 Abbott, P.M., Austin, W.E.N., Davies, S.M., Pearce, N.J.G., Hibbert, F.D., 2013.  
851 Cryptotephrochronology of a North East Atlantic marine sequence over Termination II, the  
852 Eemian and the last interglacial-glacial transition. *Journal of Quaternary Science* 28, 501-514.

853

854 Abbott, P.M., Austin, W.E.N., Davies, S.M., Pearce, N.J.G., Rasmussen, T.L., Wastegård, S.,  
855 Brendryen, J., 2014. Re-evaluation and extension of the MIS 5 tephrostratigraphy of the  
856 Faroe Islands Region: the cryptotephra record. *Palaeogeography, Palaeoclimatology,*  
857 *Palaeoecology* 409, 153-168.

858

859 Abbott, P.M., Bourne, A.J., Purcell, C.S., Davies, S.M., Scourse, J.D., Pearce, N.J.G., 2016.  
860 Last Glacial Period Cryptotephra Events in an Eastern North Atlantic Ocean Marine  
861 Sequence: Exploring Linkages to the Greenland Ice-Cores. *Quaternary Geochronology* 31,  
862 62-76.

863

864 Abbott, P.M., Davies, S.M., Austin, W.E.N., Pearce, N.J.G., Hibbert, F.D., 2011.  
865 Identification of cryptotephra horizons in a North East Atlantic marine record spanning  
866 marine isotope stages 4 and 5a (~60,000-82,000 a b2k). *Quaternary International* 246, 177-  
867 189.

868

869 Abbott, P.M., Griggs, A.J., Bourne, A.J., Chapman, M.R., Davies, S.M., submitted. Tracing  
870 marine cryptotephra in the North Atlantic during the Last Glacial Period: Improving the  
871 North Atlantic marine tephra framework. Submitted to *Quaternary Science Reviews*.

872

873 Austin, W.E.N., Wilson, L.J., Hunt, J.B., 2004. The age and chronostratigraphical  
874 significance of North Atlantic Ash Zone II. *Journal of Quaternary Science* 19, 137-146.

875

876 Berger, W., Heath, G.R., 1968. Vertical mixing in pelagic sediments. *Journal of Marine*  
877 *Research* 26, 135-143.

878

879 Bigg, G.R., Wadley, M.R., Stevens, D.P., Johnson, J.A., 1996. Prediction of iceberg  
880 trajectories for the North Atlantic and Arctic Oceans. *Geophysical Research Letters* 23, 3587-  
881 3590.

882

883 Blockley, S.P.E., Edwards, K.J., Schofield, J.E., Pyne-O'Donnell, S.D.F., Jensen, B.J.L.,  
884 Matthews, I.P., Cook, G.T., Wallace, K.L., Froese, D., 2015. First evidence of cryptotephra  
885 in palaeoenvironmental records associated with Norse occupation sites in Greenland.  
886 *Quaternary Geochronology* 27, 145-157.

887

888 Blockley, S.P.E., Pyne-O'Donnell, S.D.F., Lowe, J.J., Matthews, I.P., Stone, A., Pollard,  
889 A.M., Turney, C.S.M., Molyneux, E.G., 2005. A new and less destructive laboratory  
890 procedure for the physical separation of distal glass tephra shards from sediments. *Quaternary*  
891 *Science Reviews* 24, 1952-1960.

892

893 Bourne, A.J., Cook, E., Abbott, P.M., Seierstad, I.K., Steffensen, J.P., Svensson, A., Fischer,  
894 H., Schupbach, S., Davies, S.M., 2015. A tephra lattice for Greenland and a reconstruction of  
895 volcanic events spanning 25-45 ka b2k. *Quaternary Science Reviews* 118, 122-141.

896

897 Brendryen, J., Haflidason, H., Sejrup, H.P., 2010. Norwegian Sea tephrostratigraphy of  
898 marine isotope stages 4 and 5: Prospects and problems for tephrochronology in the North  
899 Atlantic region. *Quaternary Science Reviews* 29, 847-864.  
900

901 Davies, S.M., 2015. Cryptotephra: the revolution in correlation and precision dating. *Journal*  
902 *of Quaternary Science* 30, 114-130.  
903

904 Davies, S.M., Abbott, P.M., Meara, Rh. H., Pearce, N.J.G., Austin, W.E.N., Chapman, M. R.,  
905 Svensson, A., Bigler, M., Rasmussen, T.L., Rasmussen, S.O., Farmer, E.J., 2014. A North  
906 Atlantic tephrostratigraphical framework for 130-60 ka b2k: new tephra discoveries, marine-  
907 based correlations, and future challenges. *Quaternary Science Reviews* 106, 101-121.  
908

909 Davies, S.M., Abbott, P.M., Pearce, N.J.P., Wastegård, S., Blockley, S.P.E., 2012. Integrating  
910 the INTIMATE records using tephrochronology: rising to the challenge. *Quaternary Science*  
911 *Reviews* 36, 11-27.  
912

913 Davies, S.M., Elmquist, M., Bergman, J., Wohlfarth, B., Hammarlund, D., 2007.  
914 *Cryptotephra sedimentation processes within two lacustrine sequences from west central*  
915 *Sweden. Holocene* 17, 319-330.  
916

917 Davies, S.M., Larsen, G., Wastegård, S., Turney, C.S.M., Hall, V.A., Coyle, L., Thordarson,  
918 T., 2010. Widespread dispersal of Icelandic tephra: how does the Eyjafjöll eruption of 2010  
919 compare to past Icelandic events? *Journal of Quaternary Science* 25, 605-611.  
920

921 Dokken, T.M., Jansen, E., 1999. Rapid changes in the mechanism of ocean convection during  
922 the last glacial period. *Nature* 401, 458-461.  
923

924 Dyke, A.S., Andrews, J.T., Clark, P.U., England, J.H., Miller, G.H., Shaw, J., Veillette, J.J.,  
925 2002. The Laurentide and Innuitian ice sheets during the Last Glacial Maximum. *Quaternary*  
926 *Science Reviews* 21, 9-31.  
927

928 Elliot, M., Labeyrie, L., Bond, G., Cortijo, E., Turon, J.-L., Tisnerat, N., Duplessy, J.-D.,  
929 1998. Millennial-scale iceberg discharges in the Irminger Basin during the last glacial period:  
930 Relationship with the Heinrich events and environmental settings. *Paleoceanography* 13, 433-  
931 446.  
932

933 Elliot, M., Labeyrie, L., Dokken, T., Manthé, S., 2001. Coherent patterns of ice-rafted debris  
934 deposits in the Nordic regions during the last glacial (10-60 ka). *Earth and Planetary Science*  
935 *Letters* 194, 151-163.  
936

937 Ezat, M.M., Rasmussen, T.L., Groeneveld, J., 2014. Persistent intermediate water warming  
938 during cold stadials in the southeastern Nordic seas during the past 65 k.y.. *Geology* 42, 663-  
939 666.  
940

941 Funder, S., Kjeldsen, K.K., Kjær, K., Ó Cofaigh, C., 2011. The Greenland Ice Sheet during  
942 the past 30,000 years: a review. In Ehlers, J., Gibbard, P., Hughes, P.D. (eds) *Quaternary*  
943 *Glaciations – Extent and Chronology: A Closer Look*, pp. 699-714.  
944

945 Gehrels, M.J., Lowe, D.J., Hazell, Z.J., Newnham, R.M., 2006. A continuous 5300-yr  
946 Holocene cryptotephrostratigraphic record from northern New Zealand and implications for  
947 tephrochronology and volcanic hazard assessment. *Holocene* 16, 173-187.  
948

949 Griggs, A.J., Davies, S.M., Abbott, P.M., Coleman, M., Palmer, A.P., Rasmussen, T.L.,  
950 Johnston, R., 2015. Visualising tephra sedimentation processes in the marine environment:  
951 the potential of X-ray microtomography. *Geochemistry, Geophysics, Geosystems* 16, doi:  
952 10.1002/2015GC006073.  
953

954 Griggs, A.J., Davies, S.M., Abbott, P.M., Rasmussen, T.L., Palmer, A.P., 2014. Optimising  
955 the use of marine tephrochronology in the North Atlantic: A detailed investigation of the  
956 Faroe Marine Ash Zones II, III and IV. *Quaternary Science Reviews* 106, 122-139.  
957

958 Gudmundsson, M.T., Sigmundsson, F., Björnsson, H., Högnadóttir, T., 2004. The 1996  
959 eruption at Gjálp, Vatnajökull ice cap, Iceland: efficiency of heat transfer, ice deformation  
960 and subglacial water pressure. *Bulletin of Volcanology* 66, 46-65.  
961

962 Hall, I.R., Colmenero-Hidalgo, E., Zahn, R., Peck, V.L., Hemming, S.R., 2011. Centennial-  
963 to millennial-scale ice-ocean interactions in the subpolar northeast Atlantic 18-41 kyr ago.  
964 *Paleoceanography* 26, PA2224.  
965

966 Hayward, C., 2012. High spatial resolution electron probe microanalysis of tephtras and melt  
967 inclusions without beam-induced chemical modification. *The Holocene* 22, 119-125.  
968

969 Hibbert, F.D., Austin, W.E.N., Leng, M.J., Gatliff, R.W., 2010. British Ice Sheet dynamics  
970 inferred from North Atlantic ice-rafted debris records spanning the last 175 000 years.  
971 *Journal of Quaternary Science* 25, 461-482.  
972

973 Hoff, U., Rasmussen, T.L., Stein, R., Ezat, M.M., Fahl, K., 2016. Sea ice and millennial-scale  
974 climate variability in the Nordic seas 90 kyr ago to present. *Nature Communications* 7:12247.  
975

976 Höskuldsson, Á., Óskarsson, N., Pedersen, R., Grönvold, K., Vogfjörð, K., Ólafsdóttir, R.,  
977 2007. The millennium eruption of Hekla in February 2000. *Bulletin of Volcanology* 70, 169-  
978 182.  
979

980 Höskuldsson, Á., Sparks, R.S.J., Carroll, M.R., 2006. Constraints on the dynamics of  
981 subglacial basalt eruptions from geological and geochemical observations at Kverkfjöll, NE-  
982 Iceland. *Bulletin of Volcanology* 68, 689-701.  
983

984 Hughes, A.L.C., Gyllencreutz, R., Lohne, Ø.S., Mangerud, J., Svendsen, J.I., 2016. The last  
985 Eurasian ice sheets – a chronological database and time-slice reconstruction, DATED-1.  
986 *Boreas* 45, 1-45.  
987

988 Jakobsson, S.P., 1979. Petrology of recent basalts of the Eastern Volcanic Zone, Iceland.  
989 *Acta Naturalia Islandia* 26, 1-103.  
990

991 Jakobsson, S.P., Jónasson, K., Sigurdsson, I.A., 2008. The three igneous rock suites of  
992 Iceland. *Jökull* 58, 117-138.  
993

994 Jennings, A.E., Grönvold, K., Hilberman, R., Smith, M., Hald, M., 2002. High-resolution  
995 study of Icelandic tephra in the Kangerlussuaq Trough, southeast Greenland, during the last  
996 deglaciation. *Journal of Quaternary Science* 17, 747-757.  
997

998 Jessen, S.P., Rasmussen, T.L., 2015. Sortable silt cycles in Svalbard slope sediments 74-0 ka.  
999 *Journal of Quaternary Science* 30, 743-753.  
1000

1001 Kaminski, E., Tait, S., Ferrucci, F., Martet, M., Hirn, B., Husson, P., 2011. Estimation of ash  
1002 injection in the atmosphere by basaltic volcanic plumes: The case of the Eyjafjallajökull 2010  
1003 eruption. *Journal of Geophysical Research* 116, B00C02.  
1004

1005 Kutzbach, J.E., Wright Jr., H.E., 1985. Simulation of the climate of 18,000 years BP: Results  
1006 for the North American/North Atlantic/European sector and comparison with the geologic  
1007 record of North America. *Quaternary Science Reviews* 4, 147-187.  
1008

1009 Lacasse, C., 2001. Influence of climate variability on the atmospheric transport of Icelandic  
1010 tephra in the subpolar North Atlantic. *Global and Planetary Change* 29, 31-55.  
1011

1012 Lane, C.S., Brauer, A., Martín-Puertas, C., Blockley, S.P.E., Smith, V.C., Tomlinson, E.L.,  
1013 2015. The Late Quaternary tephrostratigraphy of annually laminated sediments from  
1014 Meerfelder Maar, Germany. *Quaternary Science Reviews* 122, 192-206.  
1015

1016 Larsen, G., Eiríksson, J., 2008. Holocene tephra archives and tephrochronology in Iceland – a  
1017 brief overview. *Jökull* 58, 229-250.  
1018

1019 Lawson, I.T., Swindles, G.T., Plunkett, G., Greenberg, D., 2012. The spatial distribution of  
1020 Holocene cryptotephra in north-west Europe since 7 ka: implications for understanding ash  
1021 fall events from Icelandic eruptions. *Quaternary Science Reviews* 41, 57-66.  
1022

1023 Le Maitre, R.W., Bateman, P., Dudek, A., Keller, J., Lameyre, Le Bas, M.J., Sabine, P.A.,  
1024 Schmid, R., Sorensen, H., Streckeisen, A., Woolley, A.R., Zanettin, B., 1989. A  
1025 Classification of Igneous Rocks and Glossary of Terms. Blackwell, Oxford.  
1026

1027 Lowe, D.J., 2011. Tephrochronology and its application: A review. *Quaternary  
1028 Geochronology* 6, 107-153.  
1029

1030 MacDonald, G.A., Katsura, T. 1964. Chemical composition of Hawaiian lavas. *Journal of  
1031 Petrology* 5, 83-133.  
1032

1033 Mackay, H., Hughes, P.D.M., Jensen, B.J.L., Langdon, P., Pyne-O'Donnell, S.D.F., Plunkett,  
1034 G., Froese, D.G., Coulter, S., Gardner, J.E., 2016. A mid to late Holocene cryptotephra  
1035 framework from eastern North America. *Quaternary Science Reviews* 132, 101-113.  
1036

1037 Mackie, E., Davies, S.M., Turney, C.S.M., Dobbyn, K., Lowe, J.J., 2002. The use of  
1038 magnetic separation techniques to detect basaltic microtephra in glacial-interglacial transition  
1039 (LGIT; 15-10 ka cal. BP) sediment sequences in Scotland. *Scottish Journal of Geology* 38,  
1040 21-30.  
1041

1042 Martrat, B., Grimalt, J.O., Shackleton, N.J., de Abreu, L., Hutterli, M.A., Stocker, T.F., 2007.  
1043 Four Climate Cycles of Recurring Deep and Surface Water Destabilizations on the Iberian  
1044 Margin. *Science* 317, 502-507.  
1045

1046 Matthews, I.P., Trincardi, F., Lowe, J.J., Bourne, A.J., Macleod, A., Abbott, P.M., Andersen,  
1047 N., Asioli, A., Blockley, S.P.E., Lane, C.S., Oh, Y.A., Satow, C.S., Staff, R.A., Wulf, S.,  
1048 2015. Developing a robust tephrochronological framework for Late Quaternary marine  
1049 records in the Southern Adriatic Sea: new data from core station SA03-11. *Quaternary*  
1050 *Science Reviews* 118, 84-104.  
1051

1052 Mayewski, P.A., Meeker, L.D., Whitlow, S., Twickler, M.S., Morrison, M.C., Bloomfield, P.,  
1053 Bond, G.C., Alley, R.B., Gow, A.J., Grootes, P.M., Meese, D.A., Ram, M., Taylor, K.C.,  
1054 Wumkes, W., 1994. Changes in Atmospheric Circulation and Ocean Ice Cover over the  
1055 North Atlantic During the last 41,000 Years. *Science* 263, 1747-1751.  
1056

1057 Obrochta, S.P., Crowley, T.J., Channell, J.E.T., Hodell, D.A., Baker, P.A., Seki, A.,  
1058 Yokoyama, Y., 2014. Climate variability and ice-sheet dynamics during the last three  
1059 glaciations. *Earth and Planetary Science Letters* 406, 198-212.  
1060

1061 Oddson, B., Gudmundsson, M.T., Larsen, G., Karlsdóttir, S., 2012. Monitoring of the plume  
1062 from the basaltic phreatomagmatic 2004 Grímsvötn eruption application of weather radar and  
1063 comparison with plume models. *Bulletin of Volcanology* 74, 1395-1407.  
1064

1065 Óladóttir, B.A., Sigmarsson, O., Larsen, G., Devidal, J.-L., 2011. Provenance of basaltic  
1066 tephra from Vatnajökull volcanoes, Iceland, as determined by major- and trace-element  
1067 analyses. *The Holocene* 21, 1037-1048.  
1068

1069 Payne, R., Gehrels, M., 2010. The formation of tephra layers in peatlands: An experimental  
1070 approach. *Catena* 81, 12-23.  
1071

1072 Peck, V.L., Hall, I.R., Zahn, R., Elderfield, H., 2008. Millennial-scale surface and sub-  
1073 surface paleothermometry from the northeast Atlantic, 55-8 ka BP. *Paleoceanography* 23,  
1074 PA3221.  
1075

1076 Peck, V.L., Hall, I.R., Zahn, R., Elderfield, H., Grousset, F., Hemming, S.R., Scourse, J.D.,  
1077 2006. High resolution evidence for linkages between NW European ice sheet instability and  
1078 Atlantic Meridional Overturning Circulation. *Earth and Planetary Science Letters* 243, 476-  
1079 488.  
1080

1081 Petersen, G.N., Bjornsson, H., Arason, P., von Löwis, S., 2012. Two weather radar time  
1082 series of the altitude of the volcanic plume during the May 2011 eruption of Grímsvötn,  
1083 Iceland. *Earth System Science Data* 4, 121-127.  
1084

1085 Pilcher, J.R., Hall, V.A., 1992. Towards a tephrochronology for the Holocene of the north of  
1086 Ireland. *The Holocene* 2, 255-259.  
1087

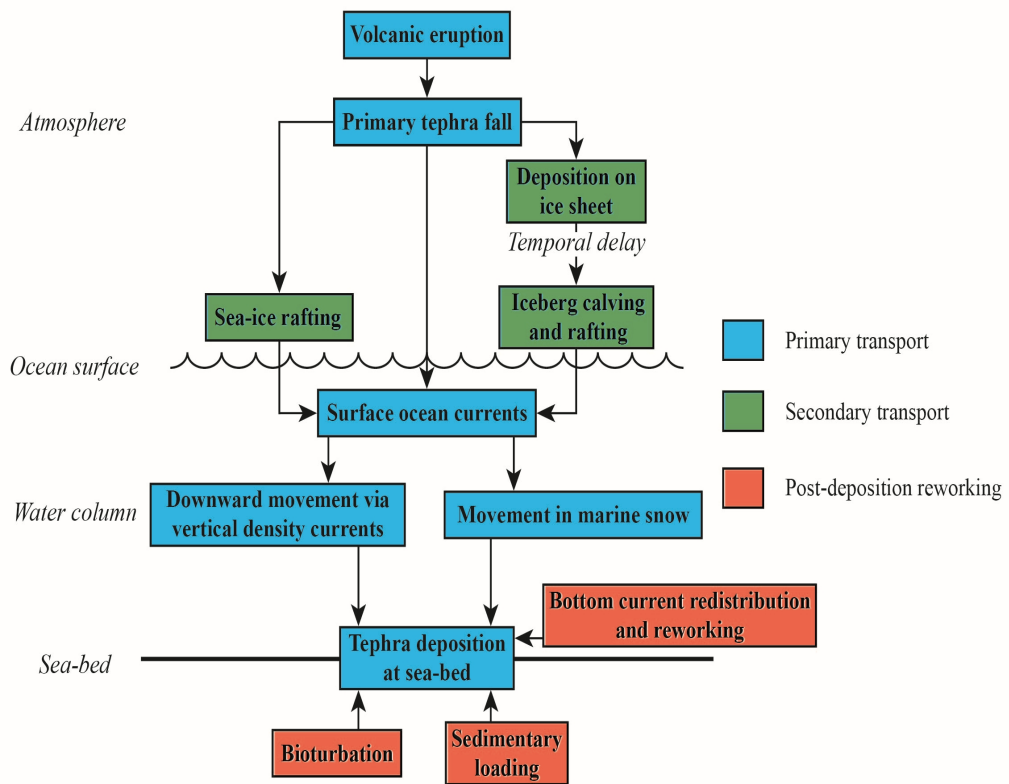
1088 Ponomareva, V., Polyak, L., Portnyagin, M., Abbott, P.M., Zelenin, E., Garbe-Schönberg, D.,  
1089 Vakhrameeva, P., (in press) "Holocene tephra from the Chukchi-Alaskan margin, Arctic  
1090 Ocean: Implications for sediment chronostratigraphy and volcanic history", *Quaternary*  
1091 *Geochronology*.

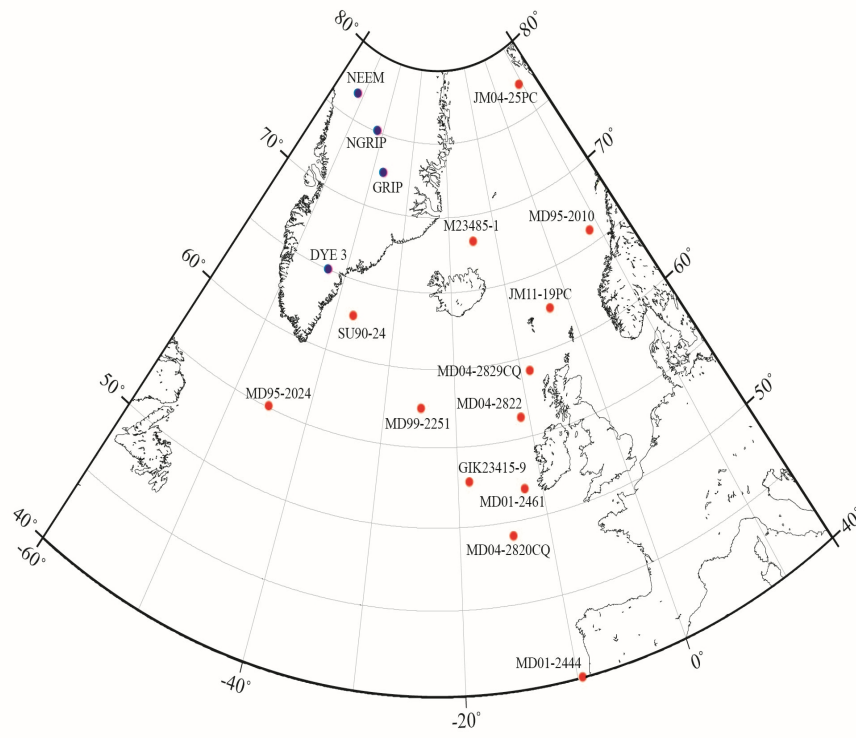
1092  
1093 Pouget, S., Bursik, M., Rogova, G., 2014. Tephra redeposition and mixing in a Lateglacial  
1094 hillside basin determined by fusion of clustering analyses of glass-shard geochemistry.  
1095 *Journal of Quaternary Science* 29, 789-802.  
1096  
1097 Pyle, D.M., 1989. The thickness, volume and grainsize of tephra fall deposits. *Bulletin of*  
1098 *Volcanology* 51, 1-15.  
1099  
1100 Pyne-O'Donnell, S.D.F., Hughes, P.D.M., Froese, D.G., Jensen, B.J.L., Kuehn, S.C., Mallon,  
1101 G., Amesbury, M.J., Charman, D.J., Daley, T.J., Loader, N.J., Mauquoy, D., Street-Perrott,  
1102 F.A., Woodman-Ralph, J., 2012. High-precision ultra-distal Holocene tephrochronology in  
1103 North America. *Quaternary Science Reviews* 52, 6-11.  
1104  
1105 Rasmussen, T.L., Thomsen, E., Moros, M., 2016. North Atlantic warming during Dansgaard-  
1106 Oeschger events synchronous with Antarctic warming and out-of-phase with Greenland  
1107 climate. *Scientific Reports* 6, 20535.  
1108  
1109 Rebesco, M., Hernandez-Molina, F., J., Van Rooij, D., Wåhlin, A., 2014. Contourites and  
1110 associated sediments controlled by deep-water circulation processes: State-of-the-art and  
1111 future considerations. *Marine Geology* 352, 111-154.  
1112  
1113 Rose, N.L., Golding, P.N.E., Batterbee, R.W., 1996. Selective concentration and enumeration  
1114 of tephra shards from lake sediment cores. *Holocene* 6, 243-246.  
1115  
1116 Ruddiman, W.F., Glover, L.K., 1972. Vertical mixing of ice-rafted volcanic ash in North  
1117 Atlantic sediments. *Geological Society Bulletin* 83, 2817-2836.  
1118  
1119 Sparks, R.S.J., Wilson, L., Sigurdsson, H., 1981. The pyroclastic deposits of the 1875  
1120 eruption of Askja, Iceland. *Philosophical Transactions of the Royal Society of London, Series*  
1121 *A* 299, 241-273.  
1122  
1123 Steinhauser, G., Bichler, M., 2008. Adsorption of ions onto high silica volcanic glass.  
1124 *Applied Radiation and Isotopes* 66, 1-8.  
1125  
1126 Stoner, J.S., Channell, J.E.T., Hillaire-Marcel, C., Kissel, C., 2000. Geomagnetic  
1127 paleointensity and environmental record from Labrador Sea core MD95-2024: global marine  
1128 sediment and ice core chronostratigraphy for the last 110 kyr. *Earth and Planetary Science*  
1129 *Letters* 183, 161-177.  
1130  
1131 Todd, J.A., Austin, W.E.N., Abbott, P.M., 2014. Quantifying bioturbation of a simulated ash  
1132 fall event. In Austin, W.E.N., Abbott, P.M., Davies, S.M., Pearce, N.J.G., Wastegård, S.,  
1133 (eds) *Marine Tephrochronology*, Geological Society of London Special Publication 398, 195-  
1134 207.  
1135  
1136 Turney, C.S.M., 1998. Extraction of rhyolitic component of Vedde microtephra from  
1137 minerogenic lake sediments. *Journal of Palaeolimnology* 19, 199-206.  
1138  
1139 Voelker, A.H.L., Haflidason, H., 2015. Refining the Icelandic tephrochronology of the last  
1140 glacial period – The deep-sea core PS2644 record from the southern Greenland Sea. *Global*  
1141 *and Planetary Change* 131, 35-62.

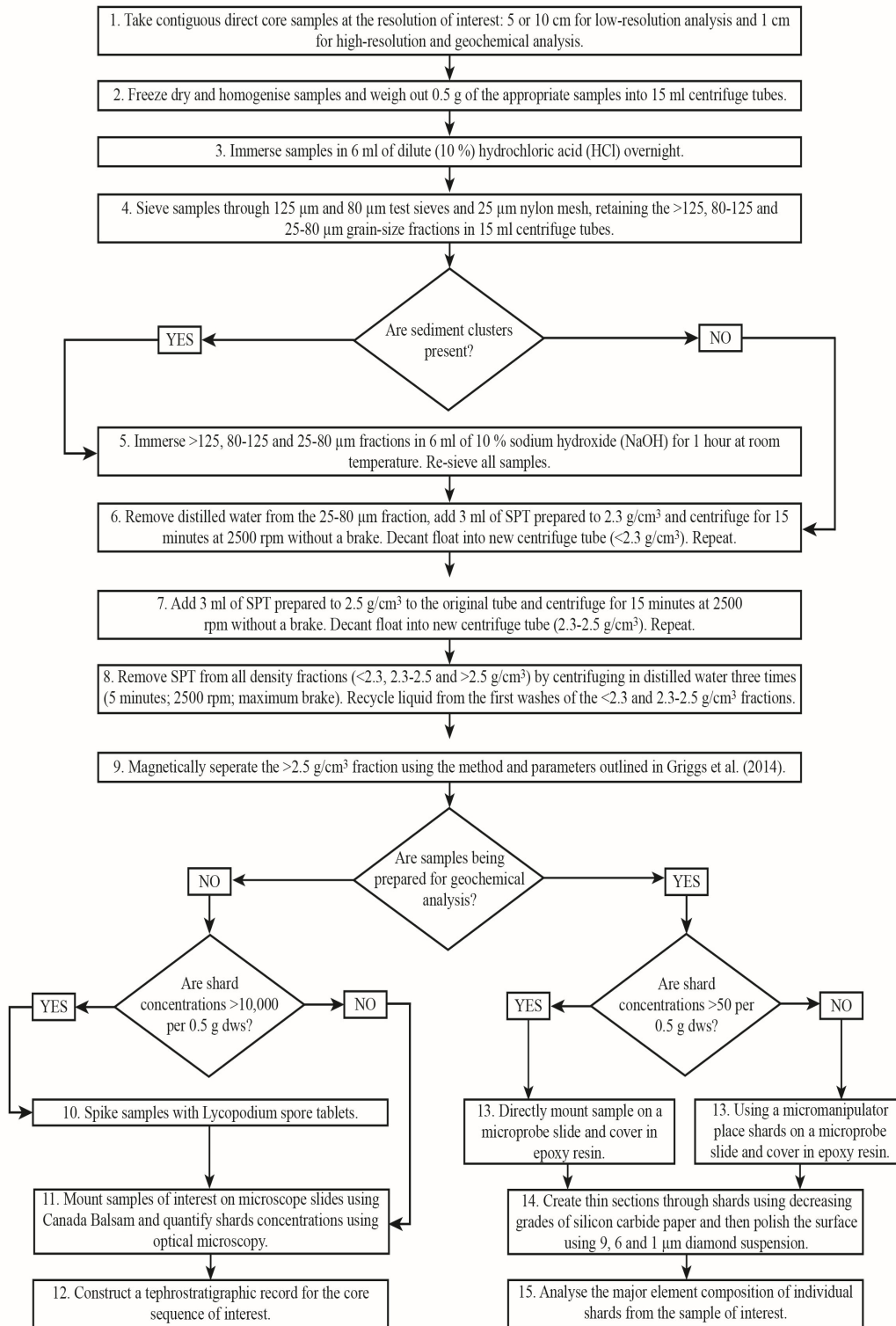
1142  
1143 Watson, E.J., Swindles, G.T., Lawson, I.T., Savov, I.P., 2015. Spatial variability of tephra  
1144 and carbon accumulation in a Holocene peatland. *Quaternary Science Reviews* 124, 248-264.  
1145  
1146 Weinelt, M., Vogelsang, E., Kucera, M., Pflaumann, U., Sarnthein, M., Voelker, A.,  
1147 Erlenkeuser, H., Malmgren, B.A., 2003. Variability of North Atlantic heat transfer during  
1148 MIS 2. *Paleoceanography* 18, 1071.  
1149



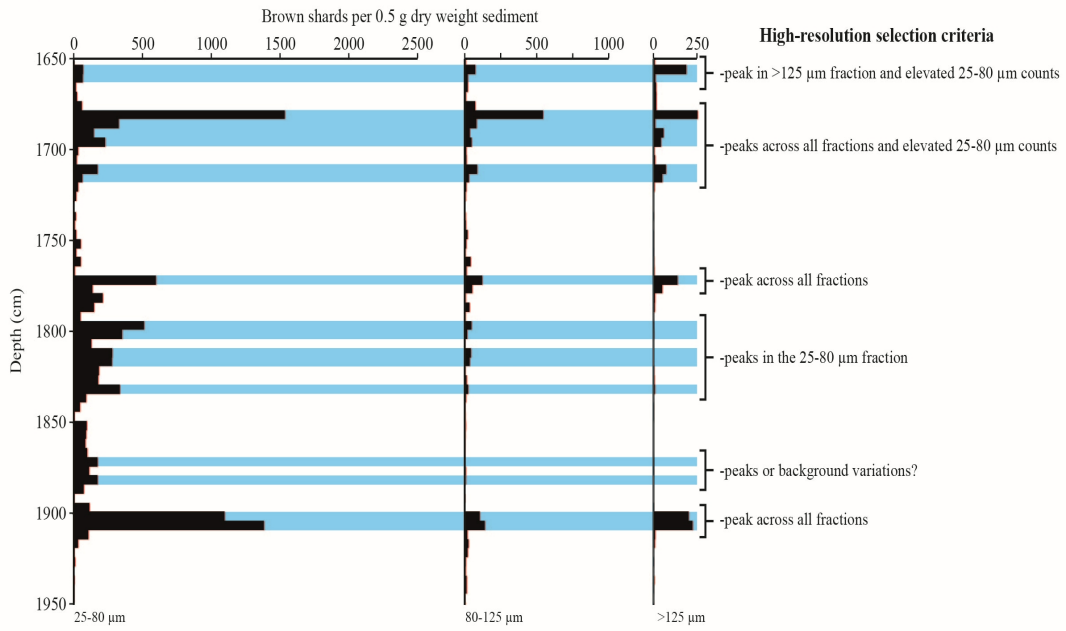




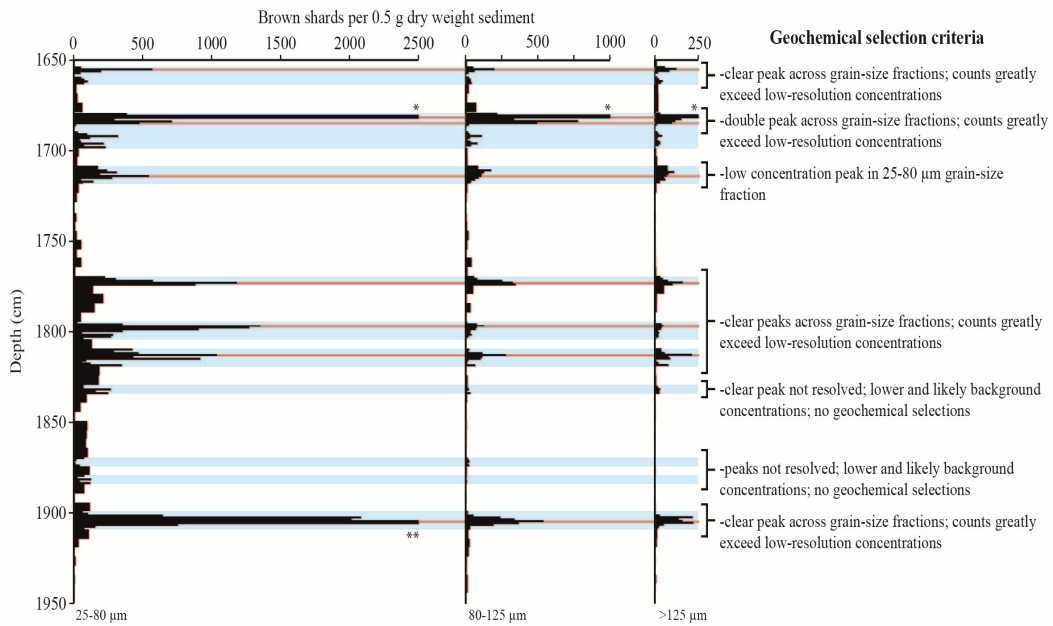




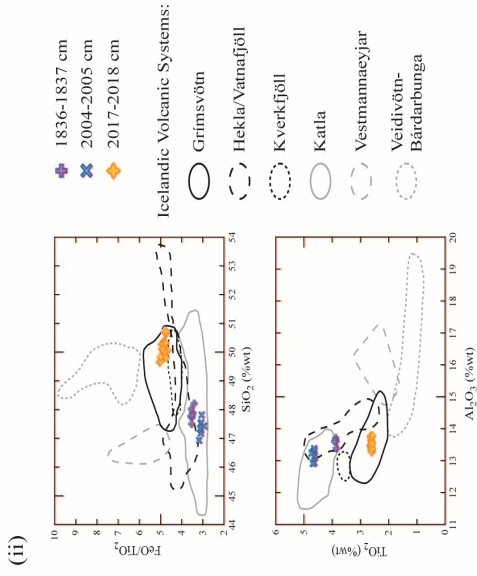
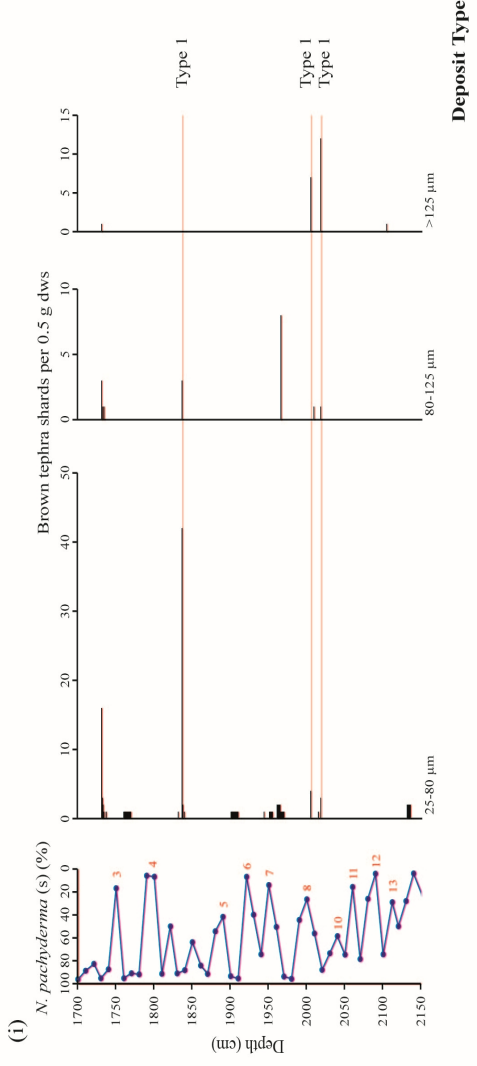
(a) Low resolution (5 cm) brown shard tephrostratigraphy for MD99-2251



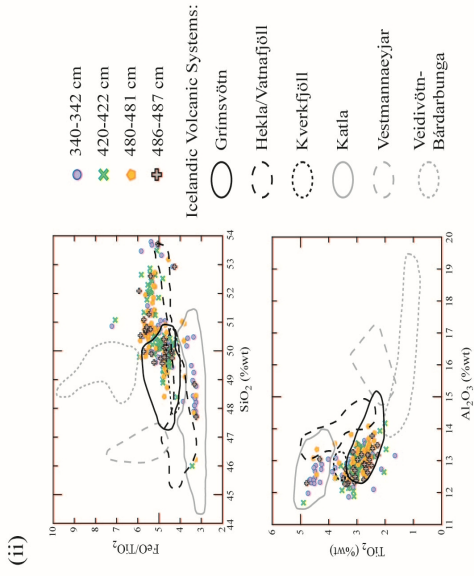
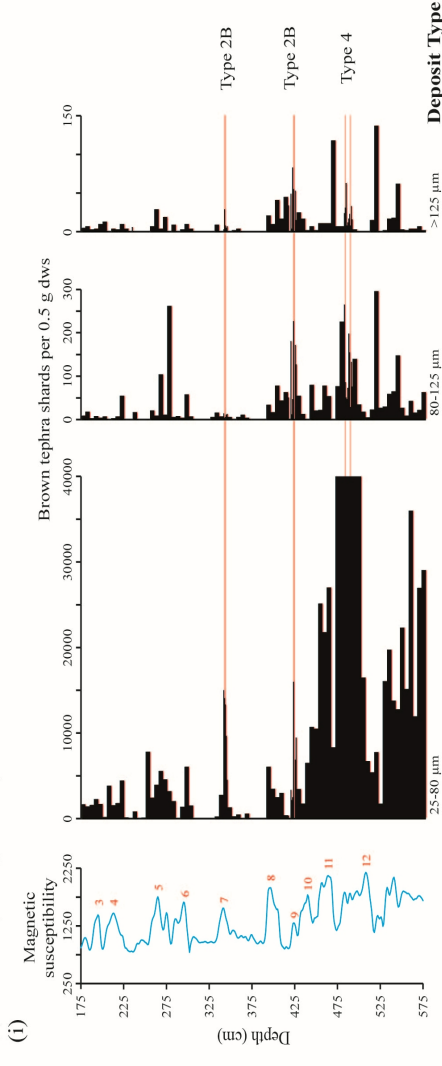
(b) Integrated high (1 cm) and low resolution (5 cm) brown shard tephrostratigraphy for MD99-2251



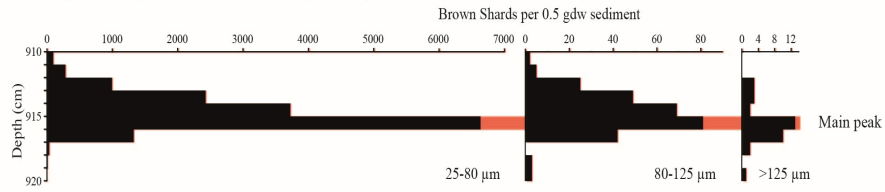
(a) MD04-2822 (Rockall Trough)



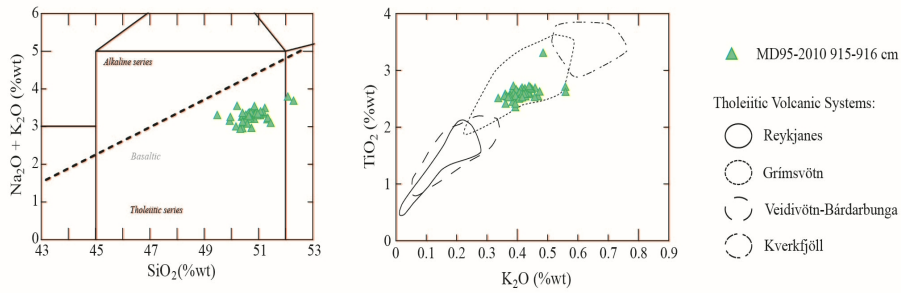
(b) SU90-24 (Irminger Basin)



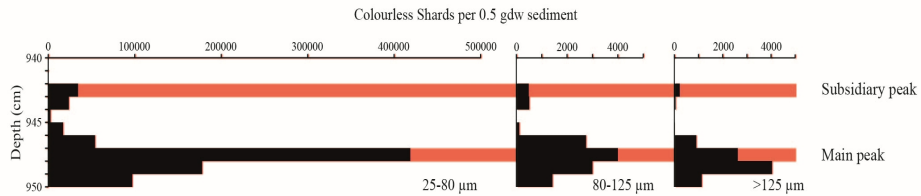
(a) (i) MD95-2010 tephrostratigraphy - 910-920 cm - Type 2A deposit example



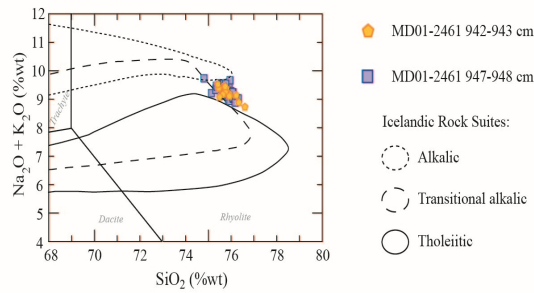
(ii) MD95-2010 915-916 cm characterisation



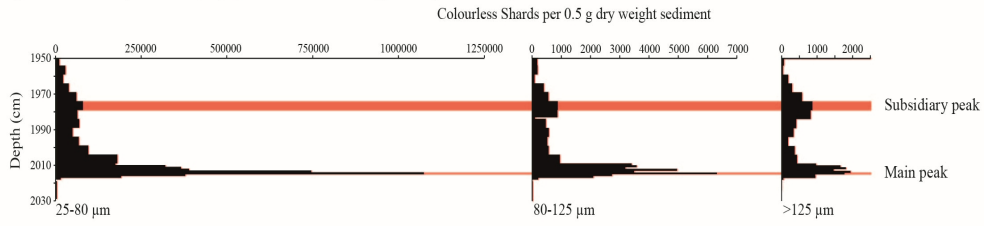
(b) (i) MD01-2461 tephrostratigraphy - 940-950 cm - Type 2A deposit example



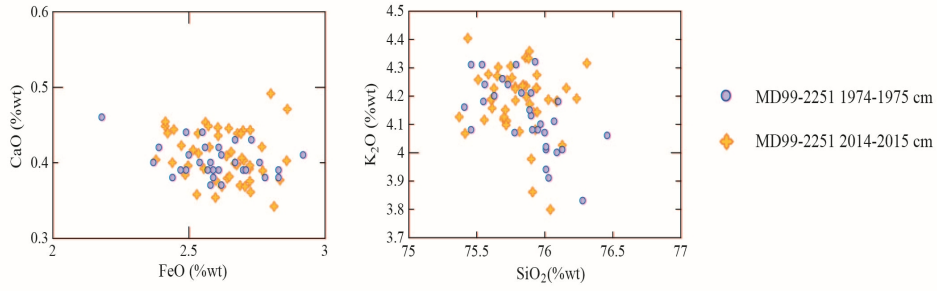
(ii) MD01-2461 947-948 cm characterisation



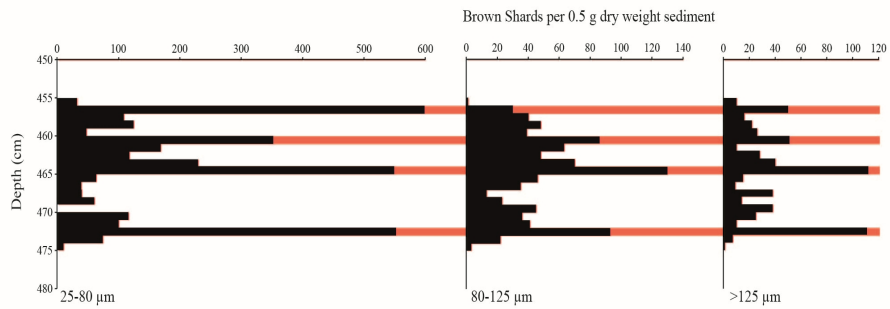
(a) (i) MD99-2251 tephrostratigraphy - 1950-2030 cm - Type 3 deposit example



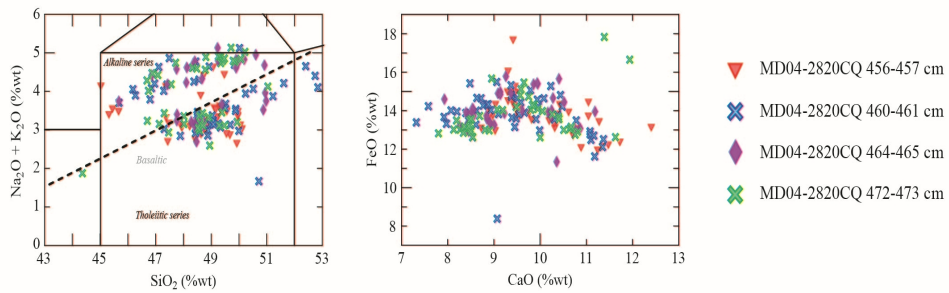
(ii) MD99-2251 1974-1975 cm and 2014-2015 cm characterisation

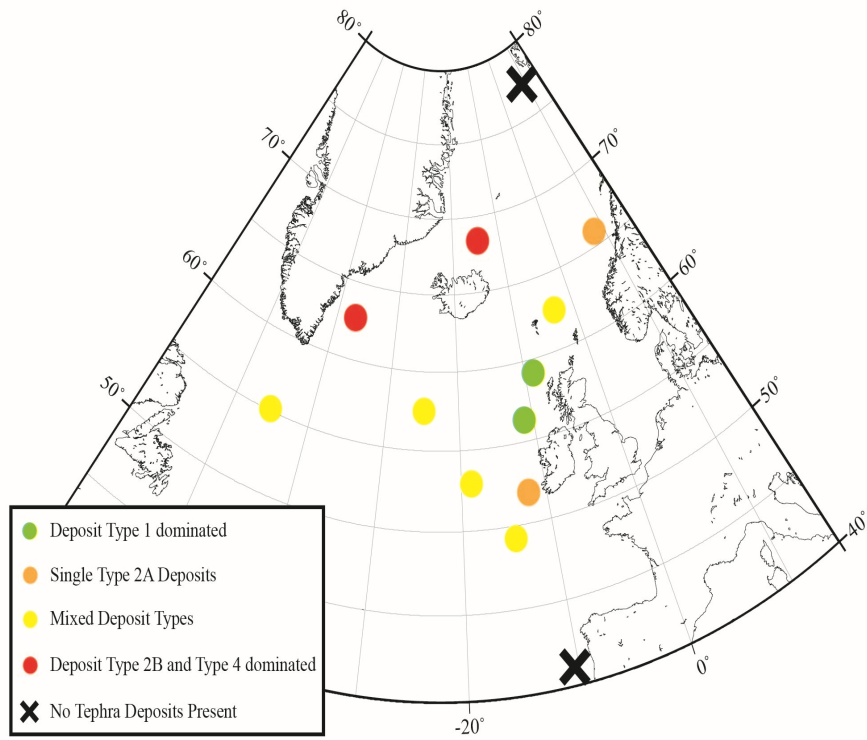


(b) (i) MD04-2820CQ tephrostratigraphy - 450-480 cm - Type 4 deposit example

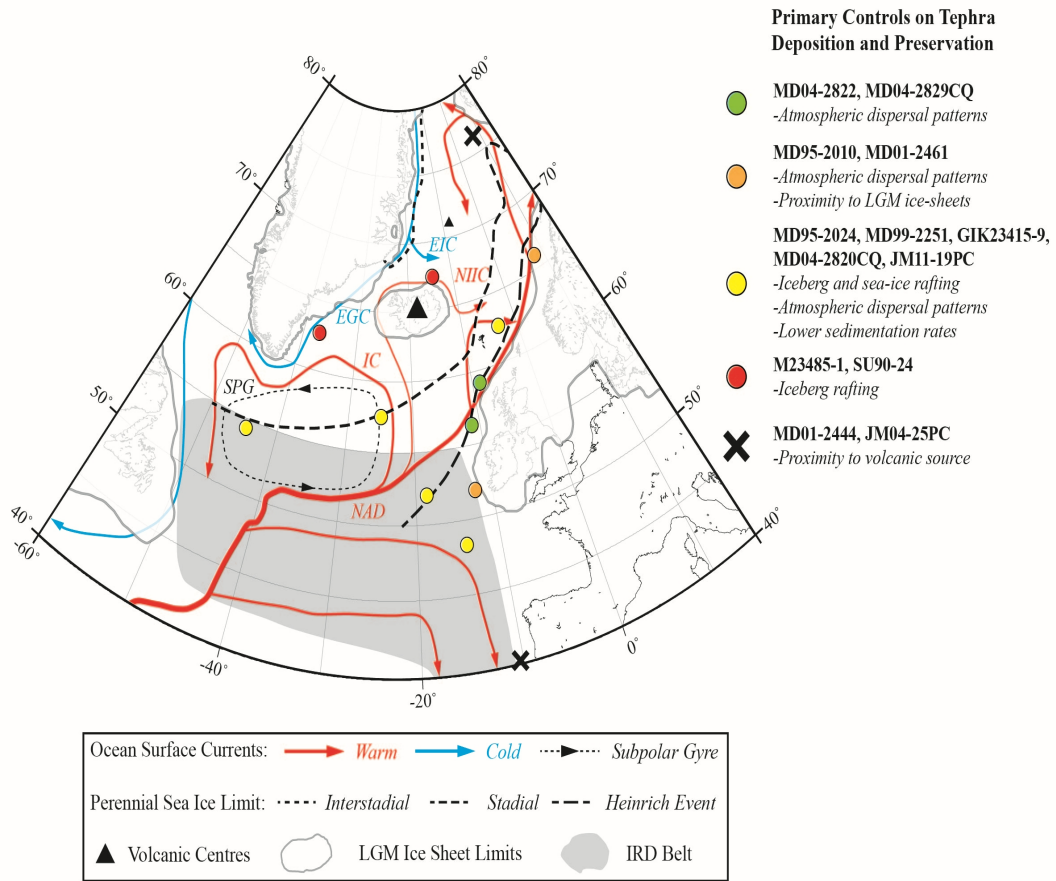


(ii) MD99-2820CQ 456-473 cm characterisation



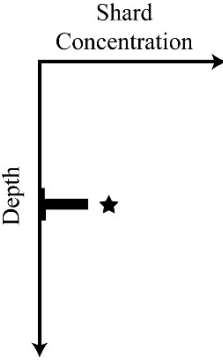
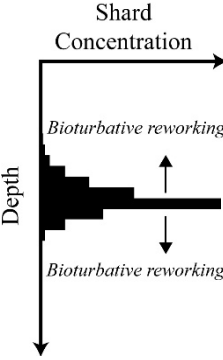
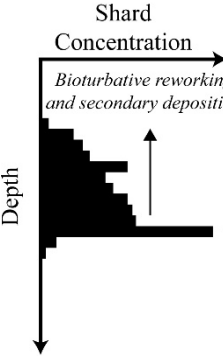
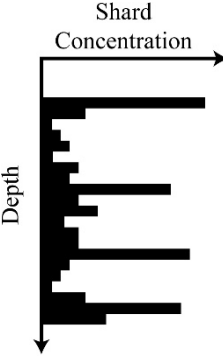
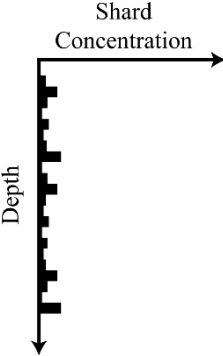






Core	Location	Lat/Long	Water Depth	Approx. Average Sedimentation Rate (cm/ka)	Example References
JM04-25PC	Western Svalbard slope	77° 28' N, 09° 30' E	1880 m	10	Jessen et al. (2015)
M23485-1	Iceland Sea	76 ° 54.9' N, 17° 52.4' W	1120 m	17	-
MD95-2010	Norwegian Sea	66° 41.05' N, 04° 33.97' E	1226 m	16	Dokken and Jansen (1999)
JM11-19PC	North Faroe Slope	62° 49' N, 03° 52' W	1179 m	11	Ezat et al. (2014); Griggs et al. (2014)
SU90-24	Irminger Basin	62° 40' N, 37° 22' W	2100 m	19	Elliot et al. (1998, 2001)
MD04-2829CQ	Rosemary Bank	58° 56.93' N, 09° 34.30' W	1743 m	20	Hall et al. (2011)
MD04-2822	Rockall Trough	56° 50.54' N, 11° 22.96' W	2344 m	14	Hibbert et al. (2010)
MD99-2251	Gardar Drift	57° 26' N, 27° 54' W	2620 m	11	-
MD95-2024	Labrador Sea	50° 12.40' N, 45° 41.22' W	3539 m	22	Stoner et al. (2000)
GIK23415-9	Northern North Atlantic	53° 10.7' N, 19° 08.7' W	2472 m	9	Weinelt et al. (2003)
MD01-2461	Porcupine Seabight	51° 45' N, 12° 55' W	1153 m	13	Peck et al. (2006, 2008)
MD04-2820CQ	Goban Spur	49° 05.29' N, 13° 25.90' W	3658 m	11	Abbott et al. (2016)
MD01-2444	Iberian Margin	37° 33.68' N, 10° 08.53' W	2637 m	23	Martrat et al. (2007)

**Table 1:** Details of the North Atlantic marine core network investigated in this study. Approximate sedimentation rates cover the 25-60 ka BP period for the cores, except for MD04-2829CQ which covers the 25-41 ka BP period, and were calculated using existing age-depth models for the sequences or approximated based on ages for event markers e.g. Heinrich events and North Atlantic Ash Zone II.

Deposit Type	Typical Shard Profile	Deposit Type Characteristics	Transport and Deposition Processes
TYPE 1 Low concentration peak		<ul style="list-style-type: none"> <li>-Well constrained shard concentration peak</li> <li>-Low shard concentrations (&lt; 50 per 0.5 g dws)</li> <li>-Shards generally 25-80 <math>\mu\text{m}</math> in diameter</li> <li>-Homogenous geochemical composition</li> </ul>	<ul style="list-style-type: none"> <li>-Single depositional event</li> <li>-Sourced from a single volcanic eruption</li> <li>-Potentially limited post-depositional reworking</li> <li>-Most likely primary airfall deposition</li> </ul>
TYPE 2 High concentration peak		<ul style="list-style-type: none"> <li>-Distinct peak in shard concentration</li> <li>-High shard concentrations (100s-1,000s per 0.5 g dws)</li> <li>-Upward and downward spanning up to 10 cm</li> <li>-Homogenous (Type 2A) or heterogeneous (Type 2B) geochemical composition</li> </ul>	<ul style="list-style-type: none"> <li>-Analysis of geochemistry, shard sizes and IRD required</li> <li>-Bioturbative reworking</li> <li>-Single depositional event</li> <li>-Transport via primary airfall, sea-ice and iceberg rafting possible</li> </ul>
TYPE 3 High concentration peak; gradational upward tail		<ul style="list-style-type: none"> <li>-Flat bottomed profile with a clear gradational upward tail</li> <li>-Very high shard concentrations (100,000s-1,000,000 per 0.5 g dws)</li> <li>-Deposit spread up to 100 cm</li> <li>-Homogenous composition of shards in peak</li> </ul>	<ul style="list-style-type: none"> <li>-Single depositional and volcanic event</li> <li>-Reworking via secondary deposition and bioturbation</li> <li>-Transport via primary airfall or sea-ice rafting</li> <li>-Useful isochron</li> </ul>
TYPE 4 Diffuse distribution; multiple peaks		<ul style="list-style-type: none"> <li>-High shard concentrations (1,000s-1,000,000s per 0.5 g dws)</li> <li>-Multiple peaks in concentration in a period of elevated shard concentrations</li> <li>-Deposit spread of 10s of cms</li> <li>-Heterogeneous geochemical composition common between peaks</li> </ul>	<ul style="list-style-type: none"> <li>-Deposition of multiple closely spaced eruptions or deposition via iceberg rafting</li> <li>-Comparison to Greenland tephra framework and IRD records required</li> <li>-Potential as regional marine-marine tie-lines</li> </ul>
TYPE 5 Background of consistent concentration		<ul style="list-style-type: none"> <li>-Consistent deposition of shards with limited variability in concentrations between samples</li> <li>-Wide variability of deposit spreads</li> <li>-Heterogeneous or geochemically related to underlying deposits</li> </ul>	<ul style="list-style-type: none"> <li>-Background signal of glass shards</li> <li>-Shards reworked and remobilised in the oceanic system</li> <li>-Potential masking of low concentration tephra deposits</li> </ul>

**Table 2:** Summary of the shard profiles, characteristics, transportation and deposition processes of tephra deposit types common to North Atlantic marine sequences between 25 and 60 ka BP. ★ = position of the isochron for that deposit type.